

# Asymptotic Distribution-free Change-point Detection for Modern Data Based on a New Ranking Scheme

Doudou Zhou and Hao Chen

**Abstract**—Change-point detection (CPD) involves identifying distributional changes in a sequence of independent observations. Among nonparametric methods, rank-based methods are attractive due to their robustness and effectiveness, and have been extensively studied for univariate data. However, they are not well explored for high-dimensional or non-Euclidean data. This paper proposes a new method, Rank INduced by Graph Change-Point Detection (RING-CPD), which utilizes graph-induced ranks to handle high-dimensional and non-Euclidean data. The new method is asymptotically distribution-free under the null hypothesis, and an analytic  $p$ -value approximation is provided for easy type-I error control. Simulation studies show that RING-CPD effectively detects change points across a wide range of alternatives and is also robust to heavy-tailed distribution and outliers. The new method is illustrated by the detection of seizures in a functional connectivity network dataset, changes in digit images, and travel pattern changes in the New York City Taxi dataset.

**Index Terms**—Graph-induced ranks; Tail probability; High-dimensional data; Network data.

## I. INTRODUCTION

Given a sequence of independent observations, an important problem is to decide whether the observations are from the same distribution or there is a change of distribution at a certain time point. Change-point detection (CPD) has attracted a lot of interest since the seminal work of [1], evolving into two primary strands: online (or sequential) CPD, which aims to detect distributional changes in real-time as data flows in (see for example [2]–[7]), and offline CPD, which involves analyzing a completely observed data sequence and is the focal point of this paper. In this big data era, CPD has diverse applications in many fields, including functional magnetic resonance recordings [8], [9], healthcare [10], [11], communication network evolution [12]–[14], and financial modeling [15], [16]. Parametric approaches (see for example, [17]–[21]) are useful to address the problem for univariate

This work of Doudou Zhou was supported in part by the NSF award DMS-1848579 and NUS Start-up Grant A-0009985-00-00. The work of Hao Chen was supported in part by the NSF awards DMS-1848579 and DMS-2311399. This paper was presented in part at the 2024 Joint Statistical Meetings (JSM) and in part at the 18th International Joint Conference on Computational and Financial Econometrics and Computational and Methodological Statistics (CFE-CMStatistics 2024). (Corresponding author: Hao Chen.)

Doudou Zhou is now with the Department of Statistics and Data Science, National University of Singapore, 117546 Singapore (e-mail: ddzhou@nus.edu.sg).

Hao Chen is now with the Department of Statistics, University of California, Davis, CA 95616 USA (e-mail: hxchen@ucdavis.edu).

and low-dimensional data, however, they are limited for high-dimensional or non-Euclidean data due to a large number of parameters to be estimated unless strong assumptions are imposed.

A few nonparametric methods have been proposed, including kernel-based methods [2], [22]–[25], interpoint distance-based methods [26], [27] and graph-based methods [28]–[36]. When dealing with high-dimensional data, the curse of dimensionality can pose a huge problem. The kernel-based method [22] assumes that the high-dimensional data resides on a low-dimensional manifold to get around this problem. On the other hand, the graph-based methods [30] incorporate a useful pattern caused by the curse of dimensionality [37], and are effective in analyzing high-dimensional and non-Euclidean data for a wide range of changes. However, the graph-based methods have focused on unweighted graphs, which may cause information loss. Later, [27] adopted a similar idea and proposed an asymptotic distribution-free approach utilizing all interpoint distances that worked well for detecting both location and scale changes. However, their test statistics are time and memory-consuming and implicitly require the existence of the second moment of the underlying distribution, which can be violated by heavy-tailed data or outliers that are common in many applications.

Among the nonparametric methods, rank-based methods are attractive for univariate data due to their robustness and effectiveness [38]–[45]. However, they are less explored for high-dimensional or non-Euclidean data. Specifically, existing multivariate rank-based methods are limited in many ways. For instance, [46] proposed to use the component-wise rank, which requires the dimension of the data to be smaller than the number of observations and suffers from dependent covariates. [47] and [48] proposed the spatial rank-based methods, which were designed mainly for detecting mean shifts. [49] proposed to use the ranks obtained from data depths, which is often used for low-dimensional data and is computationally intensive when the dimension is high.

Noticing the gap between the potential benefit of the rank-based method and the scarce exploration for multivariate/high-dimensional data, we propose a new rank-based method called **Rank INduced by Graph Change-Point Detection (RING-CPD)**, which can be applied to high-dimensional and non-Euclidean data. Unlike previous works dealing with the ranks of observations that are often limited to low-dimensional distributions, we propose to use the rank induced by similarity graphs that can be applied to data whose dimension could be

much larger than the sample size. The graph-induced rank [50] is the rank defined in the similarity graphs. Instead of treating all edges in the graph equally, we assign the rank as weights to each edge and construct the scan statistic based on the ranks. Discussions on this rank and the new test are presented in Section II. We prove that the proposed scan statistic is asymptotically distribution-free, facilitating its usage to a broader community of researchers and analysts. They are also consistent against all types of changes under certain conditions of the similarity graph (Section III). The proposed statistic can work for a wide range of alternatives and is robust to heavy-tailed distributions and outliers, as illustrated by extensive simulation studies in Section IV and three real data examples in Section V. The details of proofs of theorems are deferred to the Supplementary Material.

## II. METHOD

For a sequence of independent  $\{y_i\}_{i=1}^n$ , we consider testing

$$H_0 : y_i \sim F_0, \quad i = 1, \dots, n$$

against the single change-point alternative

$$H_1 : \exists 1 \leq \tau < n, y_i \sim \begin{cases} F_0, & i \leq \tau, \\ F_1, & \text{otherwise} \end{cases} \quad (1)$$

or the changed interval alternative

$$H_2 : \exists 1 \leq \tau_1 < \tau_2 \leq n, y_i \sim \begin{cases} F_1, & i \in [\tau_1 + 1, \tau_2] \\ F_0, & \text{otherwise,} \end{cases} \quad (2)$$

where  $F_0$  and  $F_1$  are two different distributions. When there are multiple change points, the two alternatives can be applied recursively. Alternatively, our method in the following can be extended similarly to [51] to accommodate multiple change-points, using the idea of wild binary segmentation [52] or seeded binary segmentation [53].

Our methodology begins by transforming the observations  $\{y_i\}_{i=1}^n$  into a graph-induced rank matrix  $\mathbf{R} = (R_{ij})_{i,j=1}^n \in \mathbb{R}^{n \times n}$ , which encapsulates the similarity between pairs of observations. Then we derive scan statistics utilizing  $\mathbf{R}$ . We follow notations in [50]. Let  $V = \{1, 2, \dots, n\}$  denote the vertex set of the  $n$  observations. A graph  $G$  on these observations is defined as  $G = (V, E)$ , where  $E \subseteq V \times V$ . We define that an edge  $(i, j) \in G$  if  $(i, j) \in E$ . For two graphs,  $G_1 = (V, E_1)$  and  $G_2 = (V, E_2)$ , sharing the same vertex set  $V$ , we define their intersection as  $G_1 \cap G_2 = (V, E_1 \cap E_2)$ , which is empty when there are no shared edges, i.e.,  $G_1 \cap G_2 = \emptyset$  if  $E_1 \cap E_2 = \emptyset$ , and their union as  $G_1 \cup G_2 = (V, E_1 \cup E_2)$ . Given  $\{y_i\}_{i=1}^n$ , we sequentially construct a series of simple similarity graphs<sup>1</sup>  $\{G_l\}_{l=0}^k$ , starting with an edgeless graph  $G_0 = (V, \emptyset)$ . The process continues with  $G_{l+1} = G_l \cup G_{l+1}^*$ , where  $G_{l+1}^* = \arg \max_{G' \in \mathcal{G}_{l+1}} \sum_{(i,j) \in G'} S(y_i, y_j)$  and  $\mathcal{G}_{l+1} = \{G' \in \mathcal{G} : G' \cap G_l = \emptyset\}$ . Here,  $\mathcal{G}$  represents a set of graphs subject to certain structural constraints, and  $S(\cdot, \cdot)$  is a similarity measure, such as  $S(y_i, y_j) = -\|y_i - y_j\|$  for Euclidean data, with  $\|\cdot\|$  denoting the Euclidean norm. This framework allows for

<sup>1</sup>A simple graph is a graph without self-loops and multiple edges between any two vertices.

the construction of various well-established similarity graphs under different constraints. For instance, both the  $k$ -nearest neighbor graph ( $k$ -NNG) and the  $k$ -minimum spanning tree ( $k$ -MST)<sup>2</sup> [54] satisfy the above definition of the sequence of graphs. For NNG, the structural constraint on  $G'$  is that each vertex  $i$  connects to exactly one other vertex. Specifically, the graph set  $\mathcal{G}$  is defined as  $\mathcal{G} = \{G' = (V, E') : \text{for each } i, \text{ there exists one and only one } j \in V \setminus \{i\} \text{ such that } (i, j) \in E'\}$ . Thus,  $G_1$  corresponds to the 1-NNG, where each vertex  $i$  connects to the vertex  $j$  with the largest similarity  $S(y_i, y_j)$  among all other observations. Similarly,  $G_l$  is the  $l$ -NNG,  $G_{l+1}^*$  is the  $(l+1)$ th NNG and  $G_{l+1}$  is the  $(l+1)$ -NNG. For  $k$ -MST, the constraint is that  $G'$  must be a tree connecting all vertices, making  $G_l$  the  $l$ -MST,  $G_{l+1}^*$  the  $(l+1)$ th MST and  $G_{l+1}$  the  $(l+1)$ -MST. An illustration of these graphs is presented in Figure 1. For more choices of graphs, one can see [50].

With  $\{G_l\}_{l=1}^k$ , the graph-induced rank matrix is defined as

$$R_{ij} = \sum_{l=1}^k \mathbb{1}((i, j) \in G_l) \text{ for } 1 \leq i, j \leq n,$$

where for an event  $A$ ,  $\mathbb{1}(A)$  is an indicator function that equals one if event  $A$  occurs, and equals zero otherwise. The graph-induced ranks impose more weights on the edges with higher similarity, thus incorporating more similarity information than the unweighted graph. In the meantime, the robustness property of the ranks makes the weights less sensitive to outliers compared to directly using distance. The behavior of the graph-induced rank matrix in the 10-NNG is illustrated in Figure 2 by simulated data. The graph-induced rank depends implicitly on  $k$ , and we will discuss its choice in Section IV-A.

*Remark 1 (Computational efficiency):* The computational complexities for constructing  $k$ -NNG and  $k$ -MST using brute-force methods are  $O(n^2 d)$  and  $O(n^2(d + \log n))$  [54], respectively. More efficient algorithms are widely used in practice. For example, the  $k$ -NNG can be computed using KD Tree [55] or Ball Tree algorithms [56], as implemented in scikit-learn [57], with a computational complexity of  $O(n \log n)$  when the dimension  $d$  is small (e.g.,  $d \leq 15$  as recommended by scikit-learn package). However, these methods face challenges due to the “curse of dimensionality.” In such cases, both their empirical and theoretical performance can degrade, and may become comparable or even worse than brute-force algorithms, as discussed in [58]. On the other hand, the approximate  $k$ -NNG offers a computational complexity of  $O(nd(\log n + k \log d))$ , even with high-dimensional data [58], [59].

After constructing the graph-induced rank matrix  $\mathbf{R}$ , we are ready to propose the test statistics. For testing the changed interval alternative  $H_2$  (2), each possible interval  $(t_1, t_2]$  for  $1 \leq t_1 < t_2 \leq n$  partitions the observations into two groups: one group containing all observations observed during  $(t_1, t_2]$ , and the other group containing all observations observed

<sup>2</sup>The MST is a spanning tree that minimizes the sum of distances of edges in the tree while connecting all observations. The  $k$ -MST is the union of the 1st, ...,  $k$ th MSTs, where the  $k$ th MST is a spanning tree that connects all observations while minimizing the sum of distances across edges excluding edges in the  $(k-1)$ -MST.

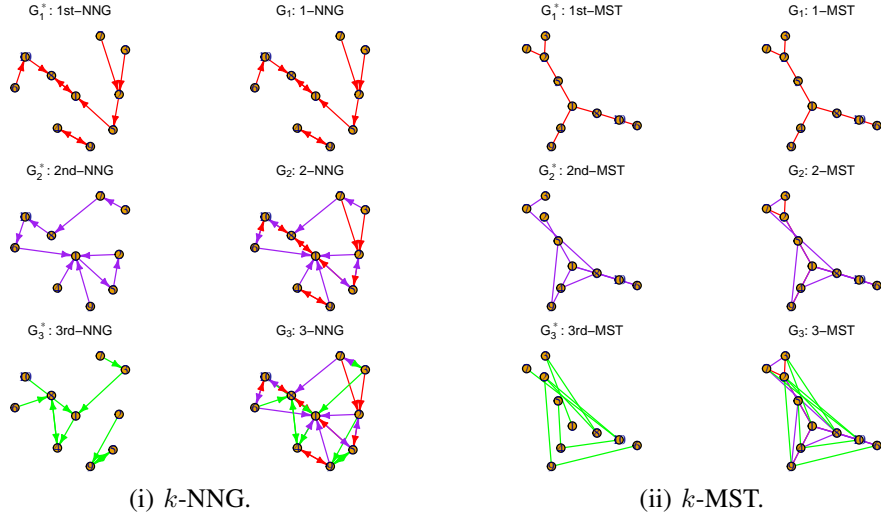


Fig. 1. Examples of different similarity graphs.

outside of this interval. Then, for any candidate changed interval  $(t_1, t_2]$ , we define two basic quantities:

$$U_1(t_1, t_2) = \sum_{i=1}^n \sum_{j=1}^n R_{ij} \mathbb{1}(t_1 < i, j \leq t_2), \quad (3)$$

$$U_2(t_1, t_2) = \sum_{i=1}^n \sum_{j=1}^n R_{ij} \mathbb{1}(i, j \leq t_1 \text{ or } i, j > t_2). \quad (4)$$

We have that  $U_1(t_1, t_2)$  is the sum of ranks within the interval  $(t_1, t_2]$ , and  $U_2(t_1, t_2)$  is the sum of ranks outside of the interval  $(t_1, t_2]$ . Then the max-type two-sample test statistic for testing the changed interval alternative can be defined as

$$M_R(t_1, t_2) = \max (Z_w(t_1, t_2), |Z_{\text{diff}}(t_1, t_2)|), \quad (5)$$

where

$$Z_w(t_1, t_2) = \frac{U_w(t_1, t_2) - \mathbb{E}(U_w(t_1, t_2))}{\sqrt{\text{Var}(U_w(t_1, t_2))}},$$

$$Z_{\text{diff}}(t_1, t_2) = \frac{U_{\text{diff}}(t_1, t_2) - \mathbb{E}(U_{\text{diff}}(t_1, t_2))}{\sqrt{\text{Var}(U_{\text{diff}}(t_1, t_2))}},$$

with  $U_{\text{diff}}(t_1, t_2) = U_1(t_1, t_2) - U_2(t_1, t_2)$  and

$$U_w(t_1, t_2) = \frac{n-t_2+t_1-1}{n-2} U_1(t_1, t_2) + \frac{t_2-t_1-1}{n-2} U_2(t_1, t_2).$$

Here we use  $\mathbb{E}$ ,  $\text{Var}$ , and  $\text{Cov}$  to respectively denote the expectation, variance, and covariance under the permutation null distribution, which places  $1/n!$  probability on each of the  $n!$  permutations of the order of the observations. Under the alternative hypothesis, it is possible that (i) both  $U_1(t_1, t_2)$  and  $U_2(t_1, t_2)$  are larger than their null expectations (a typical scenario under location alternatives) and (ii) one of them is larger than while the other one is smaller than its corresponding null expectation (a typical scenario under scale alternatives). See [37] for more discussions on these scenarios. For (i),  $Z_w(t_1, t_2)$  will be large and for (ii),  $|Z_{\text{diff}}(t_1, t_2)|$  will be large. Thus,  $M_R$  is powerful for different types of alternatives.

When testing the single change-point alternative  $H_1$  (1), we can simply use  $M_R(t) = M_R(0, t)$ . To illustrate the

behaviors of  $Z_w$ ,  $Z_{\text{diff}}$  and  $M_R$  under different scenarios, we generate  $n = 200$  independent multivariate observations with dimension  $d = 500$  from

- (a) (Null)  $y_i \sim N(\mathbf{0}_d, \mathbf{I}_d)$ ,  $i = 1, \dots, n$ ;
- (b) (Location shift)  $y_i \sim N(\mathbf{0}_d, \mathbf{I}_d)$ ,  $i = 1, \dots, 3n/4$ ,  $y_i \sim N(0.21\mathbf{1}_d, \mathbf{I}_d)$ ,  $i = 3n/4 + 1, \dots, n$ ;
- (c) (Scale shift)  $y_i \sim N(\mathbf{0}_d, \mathbf{I}_d)$ ,  $i = 1, \dots, n/4$ ,  $y_i \sim N(\mathbf{0}_d, 1.2\mathbf{I}_d)$ ,  $i = n/4 + 1, \dots, n$ ;
- (d) (Location and scale mixed shift)  $y_i \sim N(\mathbf{0}_d, \mathbf{I}_d)$ ,  $i = 1, \dots, n/2$ ,  $y_i \sim N(0.1\mathbf{1}_d, 1.2\mathbf{I}_d)$ ,  $i = n/2 + 1, \dots, n$ .

For all numeric experiments in the paper, we use the negative Euclidean norm as the similarity measure unless specifically noted. The values of  $Z_w(t) = Z_w(0, t)$ ,  $|Z_{\text{diff}}(t)| = |Z_{\text{diff}}(0, t)|$  and  $M_R(t)$  against  $t$  are presented in Figure 2.

Although the similarity measure  $S$  inherently exhibits symmetry, the rank matrix  $\mathbf{R}$  may not always maintain this property, particularly in scenarios where the graph is directed such as the  $k$ -NNG. For simplicity, we symmetrize  $\mathbf{R}$  by  $0.5(\mathbf{R} + \mathbf{R}^T)$ . Note that this symmetrization does not change the value of  $U_1$  and  $U_2$ . Without further specialization, we use  $\mathbf{R}$  to denote its symmetrized version in the following. The explicit expressions of  $\mathbb{E}(U_1(t_1, t_2))$ ,  $\mathbb{E}(U_2(t_1, t_2))$  and  $\Sigma(t_1, t_2)$  are presented in Lemma 1. Let

$$\bar{R}_{i \cdot} = \frac{\sum_{j=1}^n R_{ij}}{n-1}, r_0 = \frac{\sum_{i=1}^n \bar{R}_{i \cdot}}{n}, r_1^2 = \frac{\sum_{i=1}^n \bar{R}_{i \cdot}^2}{n},$$

$$r_d^2 = \frac{\sum_{i=1}^n \sum_{j=1}^n R_{ij}^2}{n(n-1)}, V_d = r_d^2 - r_0^2, V_r = r_1^2 - r_0^2.$$

**Lemma 1:** Under the permutation null distribution, we have

$$\mathbb{E}(U_1(t_1, t_2)) = (t_2 - t_1)(t_2 - t_1 - 1)r_0,$$

$$\mathbb{E}(U_2(t_1, t_2)) = (n - t_2 + t_1)(n - t_2 + t_1 - 1)r_0$$

$$\text{Var}(U_1(t_1, t_2)) = f_1(t_2 - t_1)V_d + f_2(t_2 - t_1)V_r,$$

$$\text{Var}(U_2(t_1, t_2)) = f_1(n - t_2 + t_1)V_d + f_2(n - t_2 + t_1)V_r,$$

$$\text{Cov}(U_1(t_1, t_2), U_2(t_1, t_2)) = f_1(t_2 - t_1)(V_d - 2(n - 1)V_r),$$

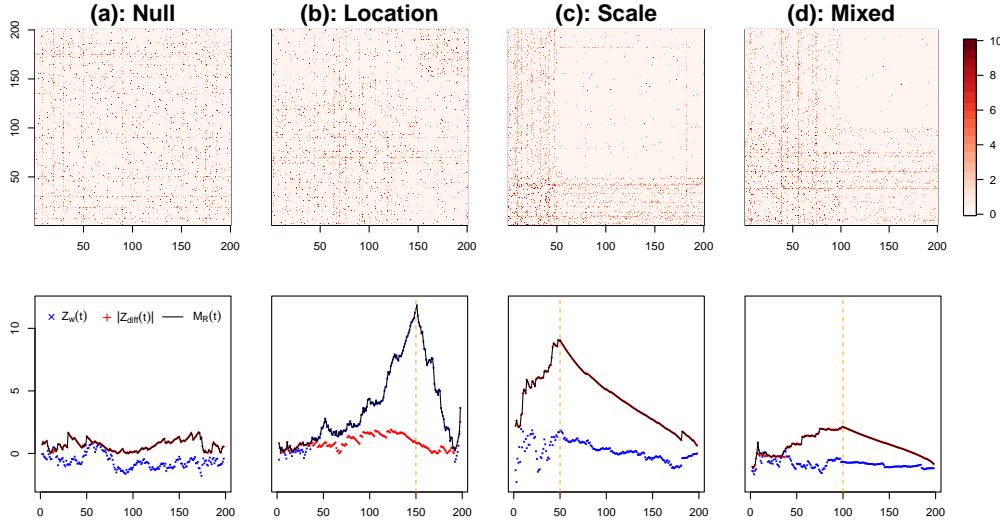


Fig. 2. Top panel: heatmap of the graph-induced rank matrix  $\mathbf{R}$  in 10-NNG. Bottom panel: the values of  $Z_w(t) = Z_w(0, t)$  (blue),  $|Z_{\text{diff}}(t)| = |Z_{\text{diff}}(0, t)|$  (red) and  $M_R(t)$  (black) against  $t$  under different scenarios. The true change points are denoted by the vertical dashed lines (orange).

where

$$f_1(t) = \frac{2t(t-1)(n-t)(n-t-1)}{(n-2)(n-3)},$$

$$f_2(t) = \frac{4t(n-t)(t-1)(t-2)(n-1)}{(n-2)(n-3)}.$$

The proof of Lemma 1 is through combinatorial analysis. It can be done similarly to the proof of Theorem 2.1 in [50] and thus omitted here. When testing against  $H_1$ , we reject  $H_0$  if the scan statistic

$$\max_{n_0 \leq t \leq n_1} M_R(t) \quad (6)$$

exceeds the critical value for a given nominal level. Here  $n_0$  and  $n_1$  are pre-specified integers. A common choice of  $n_0$  and  $n_1$  is  $n_0 = [0.05n]$  and  $n_1 = n - n_0$ , where  $[x]$  denotes the integer closest to  $x$ . When  $H_0$  is rejected, the change-point is estimated by

$$\hat{\tau} = \arg \max_{n_0 \leq t \leq n_1} M_R(t).$$

When testing against  $H_2$ , we reject  $H_0$  if the scan statistic

$$\max_{\substack{1 \leq t_1 < t_2 \leq n \\ n_0 \leq t_2 - t_1 \leq n_1}} M_R(t_1, t_2) \quad (7)$$

exceeds the critical value for a given nominal level. When  $H_0$  is rejected, the detected changed interval is

$$(\hat{\tau}_1, \hat{\tau}_2) = \arg \max_{\substack{1 \leq t_1 < t_2 \leq n \\ n_0 \leq t_2 - t_1 \leq n_1}} M_R(t_1, t_2).$$

*Remark 2:* Change-point detection is closely related to two-sample hypothesis testing. Our proposed methods utilize two-sample test statistics  $M_R$ ,  $Z_w$ ,  $Z_{\text{diff}}$  introduced in a prior work [50]. However, change-point detection is significantly more complicated. For two-sample hypothesis testing, the group labels of the observations are provided. In contrast, for change-point detection, this information is unavailable due to the unknown change-point location. In fact, even the existence of a change-point or not is unknown. Here, we use

the maximum of the scan statistic as the test statistic; that is, we compute the two-sample test statistic for each potential change-point location, and we reject the null hypothesis of no change point if any of these statistics exhibit sufficient evidence. Understanding the distribution of the scan statistic is considerably more complicated than its corresponding quantity under the two-sample testing framework. We examine the asymptotic distribution of the scan statistic in Section III.

### III. ASYMPTOTIC PROPERTIES OF THE SCAN STATISTICS

For decision-making, the critical values should be determined. Alternatively, we consider the tail probabilities

$$\mathbb{P}\left(\max_{n_0 \leq t \leq n_1} M_R(t) > b\right) \quad (8)$$

for the single change-point alternative and

$$\mathbb{P}\left(\max_{\substack{1 \leq t_1 < t_2 \leq n \\ t_0 \leq t_2 - t_1 \leq t_1}} M_R(t_1, t_2) > b\right) \quad (9)$$

for the changed interval alternative, respectively, where  $\mathbb{P}$  denotes the probability under the permutation null distribution. When  $n$  is small, we can apply the permutation procedure. However, it is time-consuming when  $n$  is large. Hence, we derive the asymptotic distribution of the scan statistics for analytic approximations of the tail probabilities.

#### A. Asymptotic null distributions of the basic processes

By the definition of  $M_R(t)$  and  $M_R(t_1, t_2)$ , it is sufficient to derive the limiting distributions of

$$\begin{aligned} & \{Z_{\text{diff}}(\lfloor nu \rfloor) : 0 < u < 1\} \text{ and} \\ & \{Z_w(\lfloor nu \rfloor) : 0 < u < 1\} \end{aligned} \quad (10)$$

for the single change-point alternative, and

$$\begin{aligned} & \{Z_{\text{diff}}(\lfloor nu \rfloor, \lfloor nv \rfloor) : 0 < u < v < 1\} \text{ and} \\ & \{Z_w(\lfloor nu \rfloor, \lfloor nv \rfloor) : 0 < u < v < 1\} \end{aligned} \quad (11)$$

for the changed-interval alternative, where  $\lfloor x \rfloor$  denotes the largest integer less than or equal to  $x$ . We use the notations  $a_n = o(b_n)$  and  $a_n \prec b_n$  when  $\lim_{n \rightarrow \infty} a_n/b_n = 0$ , and  $a_n \lesssim b_n$  when  $\lim_{n \rightarrow \infty} a_n/b_n$  is bounded. The proof of Theorem 1 is provided in Supplement S1.

**Theorem 1:** Under Conditions (1)  $r_1 \prec r_d$ ; (2)  $\sum_{i=1}^n (\sum_{j=1}^n R_{ij}^2)^2 \lesssim n^3 r_d^4$ ; (3)  $\sum_{i=1}^n |\tilde{R}_{i\cdot}|^3 \prec (nV_r)^{1.5}$ ; (4)  $\sum_{i=1}^n \tilde{R}_{i\cdot}^3 \prec nr_d V_r$ ; (5)  $|\sum_{i=1}^n \sum_{j \neq s}^n R_{ij} R_{is} \tilde{R}_{j\cdot} \tilde{R}_{s\cdot}| \prec n^3 r_d^2 V_r$ ; (6)  $\sum_{i=1}^n \sum_{j=1}^n \sum_{s, l \neq i, j} R_{ij} R_{js} R_{sl} R_{li} \prec n^4 r_d^4$ , when  $n \rightarrow \infty$ , we have

- 1)  $\{Z_{\text{diff}}(\lfloor nu \rfloor) : 0 < u < 1\}$  and  $\{Z_w(\lfloor nu \rfloor) : 0 < u < 1\}$  converge to independent Gaussian processes in finite-dimensional distributions, which we denote as  $\{Z_{\text{diff}}^*(u) : 0 < u < 1\}$  and  $\{Z_w^*(u) : 0 < u < 1\}$ , respectively.
- 2)  $\{Z_{\text{diff}}(\lfloor nu \rfloor, \lfloor nv \rfloor) : 0 < u < v < 1\}$  and  $\{Z_w(\lfloor nu \rfloor, \lfloor nv \rfloor) : 0 < u < v < 1\}$  converge to independent two-dimension Gaussian random fields in finite dimensional distributions, which we denote as  $\{Z_{\text{diff}}^*(u, v) : 0 < u < v < 1\}$  and  $\{Z_w^*(u, v) : 0 < u < v < 1\}$ , respectively.

**Remark 3:** Conditions (1)-(6) put restrictions on the similarity graph and the ranks. Importantly, they require that there should not be an excessive number of hub nodes in the graph and that the variation of the average row-wise ranks,  $V_r$ , should not be dominated by a small portion of elements. Specifically, when the largest degree of  $G_k$  is bounded by  $Ck$  for some constant  $C$ , Conditions (1), (2), (4), and (6) always hold for  $k$ -NNG and  $k$ -MST, and Conditions (3) and (5) also tend to be satisfied as verified by simulation studies. More detailed discussions can be found in Appendix E of [50]. Note that these conditions are the same as [50], which is exciting because we do not need extra conditions when we extend the statistics from the two-sample setting to the change-point detection setting.

Let  $\rho_w^*(u, v) = \text{Cov}(Z_w^*(u), Z_w^*(v))$  and  $\rho_{\text{diff}}^*(u, v) = \text{Cov}(Z_{\text{diff}}^*(u), Z_{\text{diff}}^*(v))$ . We present explicit formulas of  $\rho_w^*(u, v)$  and  $\rho_{\text{diff}}^*(u, v)$  in Theorem 2 with the proof in Supplement S2.

**Theorem 2:** The exact expressions for  $\rho_{\text{diff}}^*(u, v)$  and  $\rho_w^*(u, v)$  are

$$\begin{aligned} \rho_w^*(u, v) &= \frac{(u \wedge v)(1 - (u \vee v))}{(u \vee v)(1 - (u \wedge v))}, \\ \rho_{\text{diff}}^*(u, v) &= \frac{(u \wedge v)(1 - (u \vee v))}{\sqrt{(u \wedge v)(1 - (u \wedge v))(u \vee v)(1 - (u \vee v))}}, \end{aligned}$$

where  $u \wedge v = \min(u, v)$  and  $u \vee v = \max(u, v)$ .

Theorems 1 and 2 together show that when  $\mathbf{R}$  satisfies Conditions (1)-(6), the limiting distributions of (10) and (11), and statistics based on (10) and (11), are independent from  $\mathbf{R}$ , thus asymptotically distribution-free.

### B. Tail probabilities

Based on Theorems 1 and 2, we are able to approximate the tail probabilities using Woodroffe's method [60], [61] and Siegmund's method [62], [63]. Specifically, following the

routine of [30], and the proof of Proposition 3.4 in [28], we can approximate the tail probabilities by

$$\mathbb{P}(\max_{n_0 \leq t \leq n_1} M_R(t) > b) \quad (12)$$

$$\begin{aligned} &\approx 1 - \mathbb{P}(\max_{n_0 \leq t \leq n_1} Z_w(t) < b) \mathbb{P}(\max_{n_0 \leq t \leq n_1} |Z_{\text{diff}}(t)| < b), \\ &\mathbb{P}(\max_{\substack{1 \leq t_1 < t_2 \leq n \\ t_0 \leq t_2 - t_1 \leq t_1}} M_R(t_1, t_2) > b) \end{aligned} \quad (13)$$

$$\begin{aligned} &\approx 1 - \mathbb{P}(\max_{t_0 \leq t_2 - t_1 \leq t_1} Z_w(t_1, t_2) < b) \\ &\quad \times \mathbb{P}(\max_{t_0 \leq t_2 - t_1 \leq t_1} |Z_{\text{diff}}(t_1, t_2)| < b), \end{aligned}$$

where

$$\mathbb{P}(\max_{n_0 \leq t \leq n_1} Z_w(t) > b) \quad (14)$$

$$\approx b\phi(b) \int_{\frac{n_0}{n}}^{\frac{n_1}{n}} h_w(n, x)\nu(b\sqrt{2h_w(n, x)/n})dx,$$

$$\mathbb{P}(\max_{t_0 \leq t_2 - t_1 \leq t_1} Z_w(t_1, t_2) > b) \quad (15)$$

$$\approx b^3\phi(b) \int_{\frac{t_0}{n}}^{\frac{t_1}{n}} \left(h_w(n, x)\nu(b\sqrt{2h_w(n, x)/n})\right)^2 (1-x)dx,$$

$$\mathbb{P}(\max_{n_0 \leq t \leq n_1} Z_{\text{diff}}(t) > b) \quad (16)$$

$$\approx b\phi(b) \int_{\frac{n_0}{n}}^{\frac{n_1}{n}} h_{\text{diff}}(n, x)\nu(b\sqrt{2h_{\text{diff}}(n, x)/n})dx,$$

$$\mathbb{P}(\max_{t_0 \leq t_2 - t_1 \leq t_1} Z_{\text{diff}}(t_1, t_2) > b) \quad (17)$$

$$\approx b^3\phi(b) \int_{\frac{t_0}{n}}^{\frac{t_1}{n}} \left(h_{\text{diff}}(n, x)\nu(b\sqrt{2h_{\text{diff}}(n, x)/n})\right)^2 (1-x)dx.$$

with

$$\begin{aligned} h_w(n, x) &= \frac{(n-1)(2nx^2 - 2nx + 1)}{2x(1-x)(nx-1)(nx-n+1)}, \\ h_{\text{diff}}(n, x) &= \frac{1}{2x(1-x)}. \end{aligned}$$

Here  $v(x)$  is approximated as  $v(x) \approx \frac{(2/x)(\Phi(x/2)-0.5)}{(x/2)\Phi(x/2)+\phi(x/2)}$  [64], where  $\Phi(\cdot)$  and  $\phi(\cdot)$  are the standard normal cumulative density function and standard normal density function, respectively.

### C. Skewness correction

As observed by [28], [30], the analytical approximations of (12) and (13) can be improved by skewness correction when  $n_0$  and  $n - n_1$  decrease. It can be seen clearly in Figure 3 that  $Z_w(t)$  and  $Z_{\text{diff}}(t)$  are more skewed toward the two ends. To be specific, instead of using (14)-(17) to approximate (12) and (13), we use

$$\begin{aligned} &\mathbb{P}(\max_{n_0 \leq t \leq n_1} Z_w(t) > b) \\ &\approx b\phi(b) \int_{\frac{n_0}{n}}^{\frac{n_1}{n}} K_w(nx)h_w(n, x)\nu(b\sqrt{2h_w(n, x)/n})dx, \end{aligned} \quad (18)$$

$$\begin{aligned} &\mathbb{P}(\max_{t_0 \leq t_2 - t_1 \leq t_1} Z_w(t_1, t_2) > b) \\ &\approx b^3\phi(b) \int_{\frac{t_0}{n}}^{\frac{t_1}{n}} \left(h_w(n, x)\nu(b\sqrt{2h_w(n, x)/n})\right)^2 (1-x)dx, \end{aligned} \quad (19)$$

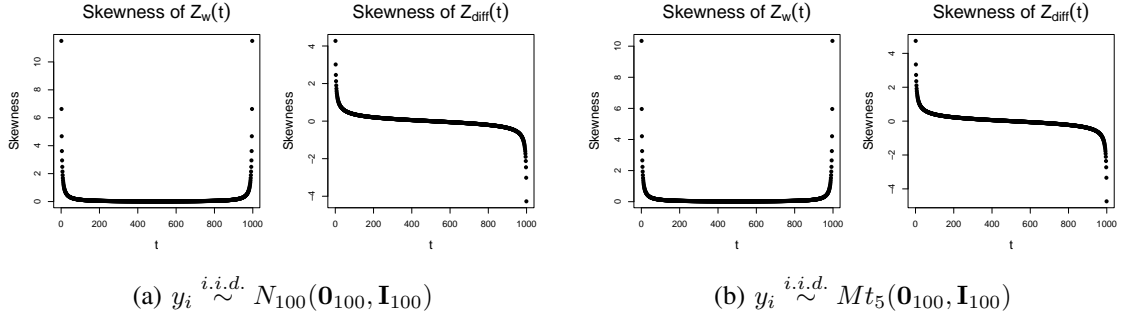


Fig. 3. Plots of skewness  $\gamma_j(t) = \mathbb{E}(Z_j^3(t))$ ,  $j = w, \text{diff}$  against  $t$  with the graph-induced rank in 10-NNG constructed on Euclidean distance on a sequence of 1000 points.

$$\mathbb{P}\left(\max_{n_0 \leq t \leq n_1} Z_{\text{diff}}(t) > b\right) \quad (20)$$

$$\approx b\phi(b) \int_{\frac{n_0}{n}}^{\frac{n_1}{n}} K_{\text{diff}}(nx) h_{\text{diff}}(n, x) \nu(b\sqrt{2h_{\text{diff}}(n, x)/n}) dx,$$

$$\mathbb{P}\left(\max_{l_0 \leq t_2 - t_1 \leq l_1} Z_{\text{diff}}(t_1, t_2) > b\right) \quad (21)$$

$$\approx b^3\phi(b) \int_{\frac{l_0}{n}}^{\frac{l_1}{n}} \left(h_{\text{diff}}(n, x) \nu(b\sqrt{2h_{\text{diff}}(n, x)/n})\right)^2 \times K_{\text{diff}}(nx)(1-x) dx,$$

where  $K_j(t) = \frac{\exp\left(\frac{1}{2}\left(b - \hat{\theta}_{b,j}(t)\right)^2 + \frac{1}{6}\gamma_j(t)\hat{\theta}_{b,j}(t)^3\right)}{\sqrt{1+\gamma_j(t)\hat{\theta}_{b,j}(t)}}$  for  $j = w, \text{diff}$ , with  $\hat{\theta}_{b,j}(t) = \frac{-1 + \sqrt{1+2\gamma_j(t)b}}{\gamma_j(t)}$  and  $\gamma_j(t) = \mathbb{E}(Z_j^3(t))$ . The only unknown quantities in the above expressions are  $\gamma_w(t)$  and  $\gamma_{\text{diff}}(t)$ , whose exact analytic expressions are quite long and are thus provided in Supplement S3.

#### D. Assessment of finite sample approximations

Here we assess the performance of the asymptotic approximations with finite samples. For a constant  $a$ , we define the first-order auto-regressive correlation matrix as  $\Sigma(a) = (a^{|i-j|})_{i,j=1}^d \in \mathbb{R}^{d \times d}$ . We consider three distributions for three different dimensions  $d = 20, 100$  and  $1000$  with  $n = 1000$ :

- (i) Multivariate Gaussian:  $y_i \sim N_d(\mathbf{0}_d, \Sigma(0.6))$ ;
- (ii) Multivariate  $t_5$ :  $y_i \sim Mt_5(\mathbf{0}_d, \Sigma(0.5))$ ;
- (iii) Multivariate log-normal:  $y_i \sim \exp(N_d(\mathbf{0}_d, \Sigma(0.4)))$ .

We report the empirical sizes estimated by 1,000 Monte Carlo simulations. Here, we focus on the graph-induced rank in  $k$ -NNG. We denote the scan statistic  $M_R(t)$  on the graph-induced rank in  $k$ -NNG by  $M_g$ -NN. We set  $n_1 = n - n_0$  and consider  $n_0 = [0.025n], [0.05n], [0.1n]$ . The nominal level is set to be 0.05. We see that the empirical sizes are well controlled across all settings even for  $n_0$  as small as  $[0.025n]$  (Table I). We further present the empirical sizes of the  $M_g$ -NN in Figure 4, considering  $k = [n^\lambda]$  with  $\lambda$  ranging from 0.2 to 0.95 in  $k$ -NNG. This visualization indicates that the empirical sizes are close to the nominal levels across a broad spectrum of  $\lambda$  values.

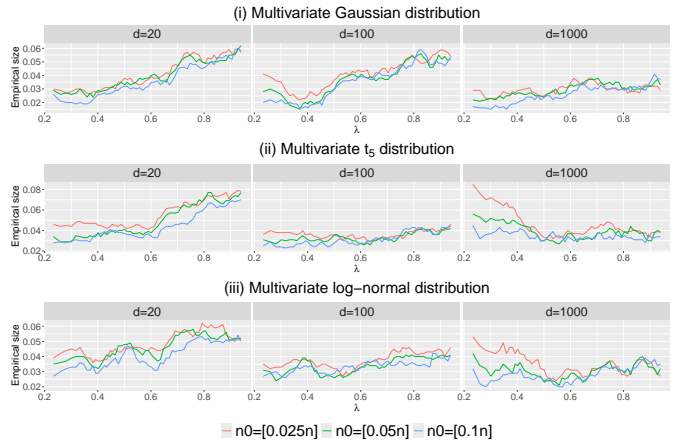


Fig. 4. Empirical size of  $M_g$ -NN after skewness correction at 0.05 nominal level with  $n = 1000$  under settings (i), (ii) and (iii). The  $k$ -NNG for  $k = [n^\lambda]$  is considered.

#### E. Consistency

We here examine the consistency of  $M_R$  when  $k$ -NNG or  $k$ -MST is used to get the graph-induced rank. At first, we define the limits

$$M(\delta_1, \delta_2) = \lim_{n \rightarrow \infty} \frac{M_R([\delta_1 n], [\delta_2 n])}{\sqrt{n}} \text{ for } 0 \leq \delta_1 < \delta_2 < 1$$

and  $M(\delta) = M(0, \delta)$  for  $0 < \delta < 1$ .

**Theorem 3:** Consider two continuous multivariate distributions  $F_0$  and  $F_1$  which differ on a set of positive Lebesgue measures and the graph-induced rank is used with  $k$ -MST or  $k$ -NNG based on the Euclidean distance, where  $k = O(1)$ .

- For the change-point alternative  $H_1$ : let  $\omega = \lim_{n \rightarrow \infty} \tau/n \in (0, 1)$ , and  $\hat{\omega} = \hat{\tau}/n$ . Assume that

$$\sup_{\delta \in (0, 1)} \left| \frac{M_R([\delta n])}{\sqrt{n}} - M(\delta) \right| \xrightarrow{P} 0 \quad (22)$$

as  $n \rightarrow \infty$ , where  $\xrightarrow{P}$  denotes the convergence in probability. Then the scan statistic of  $M_R(t)$  is consistent in that it will reject  $H_0$  against  $H_1$  with probability going to one for any significance level  $0 < \alpha < 1$  and

$$\mathbb{P}(|\hat{\omega} - \omega| > \epsilon) \rightarrow 0 \text{ as } n \rightarrow \infty \text{ for any } \epsilon > 0.$$

TABLE I  
EMPIRICAL SIZE OF  $M_g$ -NN AFTER SKEWNESS CORRECTION AT 0.05 NOMINAL LEVEL WITH  $n = 1000$  UNDER SETTINGS (I), (II) AND (III). THE  $k$ -NNG FOR VARIOUS  $k$ 'S IS CONSIDERED. HERE  $k_1 = [n^{0.5}]$ ,  $k_2 = [n^{0.65}]$  AND  $k_3 = [n^{0.8}]$ .

Setting	$d$	$n_0 = [0.1n]$			$n_0 = [0.05n]$			$n_0 = [0.025n]$		
		20	100	1000	20	100	1000	20	100	1000
(i)	5	0.04	0.02	0.02	0.04	0.03	0.02	0.05	0.04	0.04
	10	0.03	0.02	0.03	0.04	0.03	0.03	0.05	0.03	0.04
	$k_1$	0.03	0.03	0.03	0.03	0.03	0.03	0.04	0.03	0.03
	$k_2$	0.03	0.03	0.03	0.04	0.03	0.03	0.04	0.03	0.03
	$k_3$	0.04	0.03	0.04	0.05	0.04	0.04	0.06	0.04	0.03
(ii)	5	0.03	0.03	0.04	0.02	0.03	0.06	0.04	0.04	0.08
	10	0.03	0.03	0.04	0.03	0.03	0.04	0.04	0.04	0.06
	$k_1$	0.04	0.03	0.03	0.04	0.03	0.03	0.04	0.04	0.03
	$k_2$	0.04	0.04	0.03	0.05	0.03	0.03	0.05	0.04	0.04
	$k_3$	0.06	0.05	0.03	0.06	0.05	0.03	0.07	0.05	0.03
(iii)	5	0.03	0.03	0.03	0.03	0.04	0.05	0.05	0.05	0.06
	10	0.03	0.04	0.03	0.03	0.04	0.04	0.05	0.04	0.05
	$k_1$	0.04	0.03	0.02	0.05	0.03	0.02	0.05	0.03	0.03
	$k_2$	0.04	0.03	0.02	0.05	0.03	0.02	0.06	0.04	0.03
	$k_3$	0.05	0.04	0.03	0.06	0.03	0.03	0.07	0.04	0.03

- For the changed interval alternative  $H_2$ : let  $\omega_i = \lim_{n \rightarrow \infty} \tau_i/n \in (0, 1)$ , and  $\hat{\omega}_i = \hat{\tau}_i/n$  for  $i = 1, 2$ . Assume that  $\omega_2 - \omega_1 > 0$  and

$$\sup_{0 < \delta_1 < \delta_2 < 1} \left| \frac{M_R([\delta_1 n], [\delta_2 n])}{\sqrt{n}} - M(\delta_1, \delta_2) \right| \xrightarrow{P} 0 \quad (23)$$

as  $n \rightarrow \infty$ , then the scan statistic of  $M_R(t_1, t_2)$  is consistent in that it will reject  $H_0$  against  $H_2$  with probability going to one for any significance level  $0 < \alpha < 1$  and

$$\mathbb{P}(\bigcup_{i=1}^2 \{|\hat{\omega}_i - \omega_i| > \epsilon\}) \rightarrow 0 \text{ as } n \rightarrow \infty \text{ for any } \epsilon > 0.$$

The proof of this theorem is provided in Supplement S4. Although Assumptions (22) and (23) are reasonable, their

verification is difficult and is left for future work. Here we check them numerically through Monte Carlo simulations. Specifically, we consider the following combinations of  $(F_0, F_1)$  with  $\omega = 0.5$  and  $d = 500$ :

- 1) Multivariate Gaussian:  $(N_d(\mathbf{0}_d, \mathbf{I}_d), N_d(0.1\mathbf{1}_d, \mathbf{I}_d))$ ;
- 2) Multivariate  $t_3$ :  $(Mt_3(\mathbf{0}_d, \mathbf{I}_d), Mt_3(0.1\mathbf{1}_d, 1.02^2 \mathbf{I}_d))$ ;
- 3) Multivariate Cauchy:  $(MC_d(\mathbf{0}_d, \mathbf{I}_d), MC_d(2\mathbf{1}_d, \mathbf{I}_d))$ .

We generate 10 independent sequences for each setting and the plots of  $M_R([\delta n])/\sqrt{n}$  against  $\delta$  for various values of  $n$  are presented Figure 5. These plots verify the assumption that  $M_R([\delta n])/\sqrt{n}$  converges when  $n \rightarrow \infty$ .

*Remark 4:* The theoretical results in Theorem 3 are derived under the assumption of  $k = O(1)$ . However, in practice,

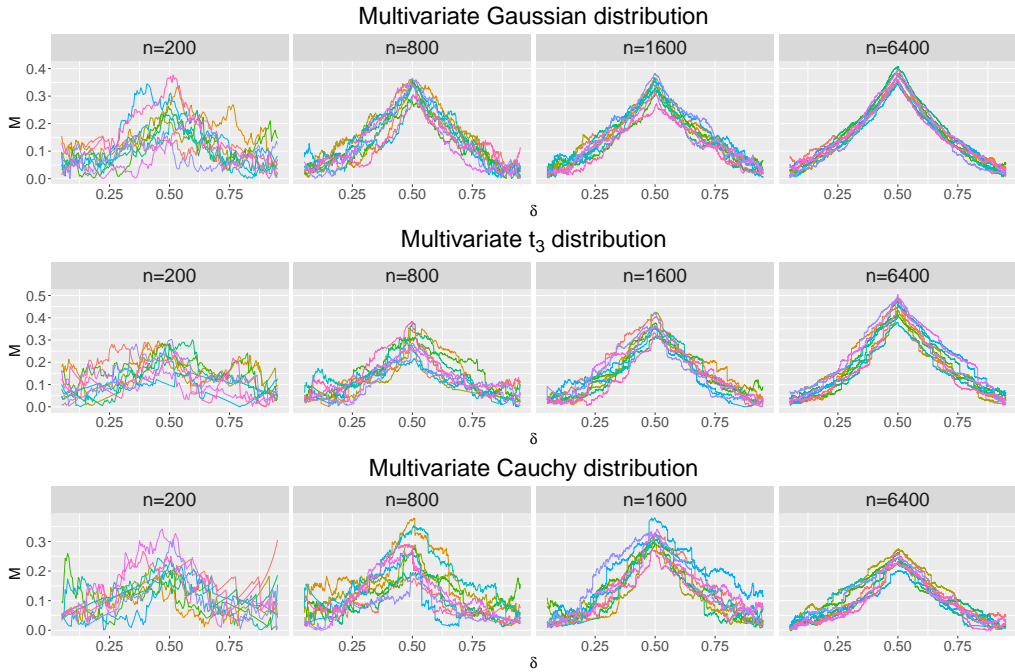


Fig. 5. Ten independent sequences (depicted using different colors) of  $M_R([\delta n])/\sqrt{n}$  against  $\delta$  for  $n = 200, 800, 1600$  and  $6400$  for the three settings.

we have observed that using larger values of  $k$ , specifically  $k = O(n^\lambda)$  for  $\lambda > 0$ , leads to increased power. This improvement can be attributed to the fact that larger  $k$  values incorporate more similarity information into the graph. Although increasing  $k$  may introduce additional noise, when  $\lambda$  is not too large, the benefits of additional similarity information outweigh the noise, compared to the case where  $k = O(1)$ . The proof of Theorem 3 builds on the foundational work by [65], which considered the minimum spanning tree, i.e.,  $k = 1$ . If a similar result to that in [65] can be established for  $k = O(n^\lambda)$  with  $\lambda > 0$ , we believe that the assumption in Theorem 3 could be relaxed to  $k = O(n^\lambda)$  as well. We leave this extension for future research.

#### IV. SIMULATION STUDIES

##### A. The choice of $k$

The choice of graphs remains an open question for CPD based on similarity graphs [28], [30], [51]. We adapt the method in [51] and [50]. Specifically, they compare the empirical power of the method for different choices of  $k = \lfloor n^\lambda \rfloor$  by varying  $\lambda$  from 0 to 1. [51] suggested using  $k = \lfloor n^{0.5} \rfloor$  for the generalized edge-count test (GET) [30] when the  $k$ -MST is used, while [50] recommended  $k = \lfloor n^{0.65} \rfloor$  for their two-sample test statistic with graph-induced rank on the  $k$ -NNG. We follow the same way in choosing  $k$  in  $M_g$ -NN. We generate independent sequences from three different distribution pairs of  $(F_0, F_1)$ :

- 1) Multivariate Gaussian:  $(N_d(\mathbf{0}_d, \mathbf{I}_d), N_d(\frac{30}{\sqrt{nd}}\mathbf{1}_d, \mathbf{I}_d))$ ;
- 2) Multivariate  $t_3$ :  $(Mt_3(\mathbf{0}_d, \mathbf{I}_d), Mt_3(\frac{30}{\sqrt{nd}}\mathbf{1}_d, (1 + \frac{30}{\sqrt{nd}})^2\mathbf{I}_d))$ ;
- 3) Multivariate Cauchy:  $(MC_d(\mathbf{0}_d, \mathbf{I}_d), MC_d(\frac{30}{\sqrt{n}}\mathbf{1}_d, \mathbf{I}_d))$ .

The parameters are chosen so that the tests have moderate power. The change-point is set to be  $\tau = n/2$ , the dimension  $d = 500$  and  $n = 50, 100, 200$ . We set  $n_0 = \lceil 0.05n \rceil$  and  $n_1 = n - n_0$ , which will also be our choice by default in latter experiments, where  $\lceil x \rceil$  denotes the smallest integer larger than or equal to  $x$ . For comparison, we also include two graph-based methods, GET and the max-type edge-count test (MET) proposed in [30] using the  $k$ -MST. The empirical power is defined as the ratio of successful detection where the  $p$ -value is smaller than 0.05. For fairness, the  $p$ -values are approximated by 1,000 random permutations for all methods.

Figure 6 illustrates the power of the tests for different values of  $k = \lfloor n^\lambda \rfloor$ . For  $M_g$ -NN,  $\lambda \in (0, 0.95]$ , while for GET and MET,  $k$  is chosen from 1 to  $\min\{\lfloor n^{0.95} \rfloor, \lfloor \frac{n-1}{2} \rfloor\}$ . This range is chosen because the  $l$ th-MST contains  $n - 1$  edges, whereas a complete graph has  $n(n - 1)/2$  edges. We observe that the power of these tests initially increases rapidly as  $k$  or  $\lambda$  increases. However, as  $k$  continues to increase, the power of GET and MET decreases sharply. In contrast,  $M_g$ -NN demonstrates greater robustness, maintaining consistent performance even for larger values of  $k$  (e.g.,  $k > n^{0.65}$ ). In the case of the multivariate Cauchy distribution, the power of  $M_g$ -NN exhibits a slight decrease when  $k > n^{0.65}$ , but overall remains stable. This robustness of  $M_g$ -NN can be attributed to its use of ranks on the edges, which effectively

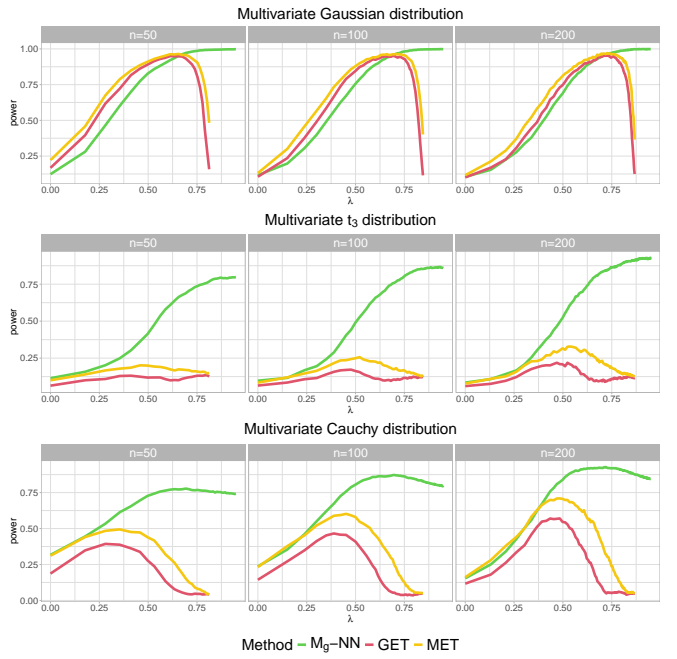


Fig. 6. Empirical power of  $M_g$ -NN, GET, and MET over 1000 times of repetitions under each setting.

reduces the impact of additional noise from denser graphs by assigning smaller ranks to edges introduced later. As a result,  $M_g$ -NN consistently achieves the best performance, showing a significant improvement in power for heavy-tailed distributions (such as the multivariate  $t_3$  and Cauchy distributions) and demonstrating resilience across a wide range of  $k$  values. Considering the trade-offs between computational cost, control of type I error, and power, we select  $\lambda = 0.65$  for  $M_g$ -NN, and  $\lambda = 0.5$  for GET and MET in subsequent analyses. These choices strike a reasonable balance and are consistent with previous recommendations [50], [51].

*Remark 5:* Selecting an appropriate value of  $k$  remains an open question for graph-based methods in real-world applications. Beyond using a fixed value, such as  $k = \lfloor n^{0.65} \rfloor$ , we propose a data-driven approach to empirically determine  $k$ . Specifically, we first randomly permute the observations, then apply a mean shift to the last  $\lceil n/2 \rceil$  observations by adding a value  $\mu$  to each dimension. We then select the  $k$  value that produces the smallest  $p$ -value. This approach incorporates the unknown underlying distribution for choosing an optimal value of  $k$ .

##### B. Performance comparison

We compare RING-CPD to GET and MET on  $k$ -MST with  $k = \lfloor n^{0.5} \rfloor$ , the graph-based method on the shortest Hamiltonian path [29] (SWR), the method based on Fréchet means and variances [66] (DM). We also compare three interpoint distance-based methods, the widely used distance-based method E-Divisive (ED) [26] implemented in the R package *ecp*, and the other two methods proposed recently by [27] and [34]. [27] proposed four statistics and we compare the statistic  $C_{2N}$  that had a satisfactory performance in most

of their simulation settings. [34] proposed three statistics, which perform well for location change, scale change, and general change, respectively. Here we compare with their statistic  $S_3$ , which they concluded to have relatively robust performance across various alternatives. For fairness, the  $p$ -values of all these methods are approximated by 1,000 random permutations.

We set  $n = 200$  and the change-point  $\tau = [n/3]$  and consider the dimension of the distributions  $d = 200, 500, 1000$ . Before the change-point  $y_i \sim F_0$  and after the change-point  $y_i \sim F_1$ . We consider both the empirical power and the detection accuracy estimated from 1000 trials for each scenario. The empirical power is the ratio of the successful detection defined as  $p$ -value smaller than the nominal level 0.05. The detection accuracy is provided in parentheses, which is the ratio of trials that the detected change-point is located in  $[\tau - 0.05n, \tau + 0.05n]$  and the  $p$ -value smaller than 0.05. We consider various settings that cover light-tailed, heavy-tailed, skewed, and mixture distributions for location, scale, and mixed alternatives. Specifically, we consider six settings for  $F_i$ ,  $i = 0, 1$ :

- (I) Multivariate Gaussian:  $N_d(\boldsymbol{\mu}_i, \boldsymbol{\Sigma}_i)$ ;
- (II) Multivariate  $t_5$ :  $Mt_5(\boldsymbol{\mu}_i, \boldsymbol{\Sigma}_i)$ ;
- (III) Multivariate Cauchy:  $MC_d(\boldsymbol{\mu}_i, \boldsymbol{\Sigma}_i)$ ;
- (IV) Multivariate  $\chi_5^2$ :  $\chi_5^2(\boldsymbol{\mu}_i, \boldsymbol{\Sigma}_i)$  (generated as  $\boldsymbol{\Sigma}_i^{\frac{1}{2}}(X - 5\mathbf{1}_d + \boldsymbol{\mu}_i)$  where the  $d$  components of  $X$  are i.i.d.  $\chi_5^2$ );
- (V) Multivariate Gaussian mixture:  $WN_d(\boldsymbol{\mu}_i, \boldsymbol{\Sigma}_i) + (1 - W)N_d(-\boldsymbol{\mu}_i, \boldsymbol{\Sigma}_i)$  with  $W \sim \text{Bernoulli}(0.5)$ ;
- (VI) Multivariate Gaussian with Multivariate  $t_7$  outliers  $WN_d(\boldsymbol{\mu}_i, \boldsymbol{\Sigma}_i) + (1 - W)Mt_7(\boldsymbol{\mu}_i, \boldsymbol{\Sigma}_i)$  with  $W \sim \text{Bernoulli}(0.9)$ .

We set  $\boldsymbol{\mu}_0 = \mathbf{0}_d$  for  $F_0$  and  $\boldsymbol{\mu}_1 = \delta\mathbf{1}_d$  for  $F_1$ , where  $\delta$  is different for different settings. For each setting, we consider five different changes:

- (a) location ( $\delta \neq 0$  and  $\boldsymbol{\Sigma}_1 = \boldsymbol{\Sigma}_0$ );
- (b) simple scale ( $\delta = 0$  and  $\boldsymbol{\Sigma}_1 = (1 + \sigma)^2\boldsymbol{\Sigma}_0$ );
- (c) complex scale ( $\delta = 0$  and  $\boldsymbol{\Sigma}_1 \neq \boldsymbol{\Sigma}_0$ );
- (d) location and simple scale mixed ( $\delta \neq 0$  and  $\boldsymbol{\Sigma}_1 = (1 + \sigma)^2\boldsymbol{\Sigma}_0$ );
- (e) location and complex scale mixed ( $\delta \neq 0$  and  $\boldsymbol{\Sigma}_1 \neq \boldsymbol{\Sigma}_0$ ).

The choice of  $\delta$ ,  $\sigma$ , and  $\boldsymbol{\Sigma}_i$ ,  $i = 1, 2$  are specified differently for the settings and alternatives, summarized in Table II, where the changes in signal are set so that the best test has moderate

power to be comparable. Here for Setting IV, the covariance matrices  $\mathbf{A}_i = \mathbf{V}\mathbf{B}_i\mathbf{V}$ , for  $i = 0, 1, 2$ , where  $\mathbf{V}$  is a diagonal matrix with the diagonal elements sampled independently from  $U(1, 3)$ ,  $\mathbf{B}_i = \text{diag}(\mathbf{B}_{i1}, \dots, \mathbf{B}_{i\frac{d}{10}})$  is a block-diagonal correlation matrix. Each diagonal block  $\mathbf{B}_{ij}$  is a  $10 \times 10$  matrix with diagonal entries being 1 and off-diagonal entries equal to  $\rho_{ij} \sim U(a_j, b_j)$  independently. We set  $a_0 = 0, b_0 = 0.5$ ,  $a_1 = 0.3, b_1 = 0.8$  and  $a_3 = 0.2, b_3 = 0.7$ . Each configuration is repeated 1,000 times. We present the results of Settings I-III in Table III, and the results of Settings IV-VI in Table IV. Under each setting, the largest value and those larger than 95% of the largest value are highlighted in bold.

For the multivariate  $t_5$  and Cauchy distributions,  $M_g$ -NN shows the highest power under the alternatives (a), (b), (d), and (e). SWR performs the best for the complex scale alternative (c), followed immediately by  $M_g$ -NN, while GET and MET also have moderate power. On the contrary, DM, ED,  $C_{2N}$  and  $S_3$  fail for most of the alternatives under the multivariate  $t_5$  and Cauchy distributions with the power close to the nominal level. It shows that  $M_g$ -NN is robust to heavy-tailed distributions, while other methods such as  $C_{2N}$  and  $S_3$  are not.

From Table IV, we see that ED and  $C_{2N}$  perform the best for the location alternative (a) under the multivariate  $\chi_5^2$  distribution, while  $M_g$ -NN performs the second best and  $S_3$  has no power. For the scale alternative (b),  $S_3$  exhibits the highest power, and  $M_g$ -NN also performs well. In addition, under the same distribution,  $M_g$ -NN and SWR outperform other methods for alternatives (c) and (e). However, SWR is powerless for alternative (d) while  $M_g$ -NN shows good performance.

For the Gaussian mixture distribution,  $C_{2N}$  has the highest power for the location alternative (a), while  $M_g$ -NN is the second best. For alternatives (b) and (d),  $M_g$ -NN has the best performance, together with GET and MET, while all other methods have unsatisfactory performance. For alternatives (c) and (e), SWR achieves the highest power, while  $M_g$ -NN is also good with performance better than other methods.

For the multivariate Gaussian distribution with  $t_7$  outliers, ED is the best for the location alternative, while for  $d = 1000$ , it is outperformed by  $M_g$ -NN in the detection accuracy. For other alternatives,  $M_g$ -NN almost dominates other methods, followed by GET and MET. It shows that  $M_g$ -NN is robust to outliers.

TABLE II  
THE SPECIFIC CHANGES FOR DIFFERENT SETTINGS AND ALTERNATIVES.

Setting	$H_0$ $\boldsymbol{\Sigma}_0$	Alternative					
		(a) $\delta$	(b) $\sigma$	(c) $\boldsymbol{\Sigma}_1$	(d) $\delta$	$\sigma$	(e) $\delta$
(I)	$\boldsymbol{\Sigma}(0.6)$	$\frac{2\log d}{5\sqrt{d}}$	$\sqrt{\frac{\log d}{16d}}$	$\boldsymbol{\Sigma}(0.16)$	$\frac{\log d}{10\sqrt{d}}$	$\sqrt{\frac{\log d}{16d}}$	$\sqrt{\frac{\log d}{4d}}$
(II)	$\boldsymbol{\Sigma}(0.6)$	$\frac{5\log d}{4\sqrt{d}}$	$\sqrt{\frac{3\log d}{10\sqrt{d}}}$	$0.6\boldsymbol{\Sigma}(0.1)$	$\frac{\log d}{3\sqrt{d}}$	$\sqrt{\frac{3\log d}{10\sqrt{d}}}$	$\frac{\log d}{2\sqrt{d}}$
(III)	$\boldsymbol{\Sigma}(0.4)$	$\frac{11\log d}{20\sqrt{d}}$	$\sqrt{\frac{6\log d}{5d^{2/5}}}$	$\boldsymbol{\Sigma}(0.85)$	$\frac{6\log d}{25d^{2/5}}$	$\sqrt{\frac{\log d}{25d}}$	$\frac{6\log d}{25d^{2/5}}$
(IV)	$\mathbf{A}_0$	$\frac{5\log d}{2\sqrt{d}}$	$\frac{9}{10\sqrt{d}}$	$\mathbf{A}_1$	$\sqrt{\frac{49\log d}{16d}}$	$\frac{3}{4\sqrt{d}}$	$\sqrt{\frac{49\log d}{16d}}$
(V)	$\mathbf{I}_d$	$\frac{3}{5\log d}$	$\sqrt{\frac{\log d}{25d}}$	$\boldsymbol{\Sigma}(0.55)$	$\frac{3}{10\log d}$	$\sqrt{\frac{\log d}{25d}}$	$\frac{3}{10\log d}$
(VI)	$\boldsymbol{\Sigma}(0.5)$	$\frac{7\log d}{20\sqrt{d}}$	$\sqrt{\frac{\log d}{5\sqrt{d}}}$	$\boldsymbol{\Sigma}(0.1)$	$\frac{\log d}{5\sqrt{d}}$	$\sqrt{\frac{\log d}{5\sqrt{d}}}$	$\frac{\log d}{5\sqrt{d}}$

TABLE III  
THE EMPIRICAL POWER (DETECTION ACCURACY) IN PERCENT UNDER SETTINGS I-III. HERE  $M_g$ -NN IS THE PROPOSED METHOD.

$d$	Setting I (Gaussian)			Setting II ( $t_5$ )			Setting III (Cauchy)		
	200	500	1000	200	500	1000	200	500	1000
(a) Location change									
$M_g$ -NN	76(58)	67(49)	59(40)	<b>89(71)</b>	<b>79(59)</b>	<b>67(49)</b>	<b>99(88)</b>	<b>91(78)</b>	<b>72(55)</b>
GET	63(46)	52(36)	40(25)	68(48)	41(26)	20(12)	85(72)	54(40)	28(17)
MET	68(50)	58(39)	46(30)	75(52)	50(32)	31(18)	90(75)	67(50)	44(26)
SWR	21(8)	18(6)	16(4)	19(6)	19(6)	15(4)	44(23)	40(18)	32(15)
DM	7(0)	6(0)	7(0)	6(0)	5(0)	4(0)	5(0)	4(0)	5(0)
ED	<b>97(85)</b>	<b>96(83)</b>	<b>95(80)</b>	73(57)	28(19)	12(4)	6(1)	5(0)	4(1)
$C_{2N}$	<b>95(81)</b>	<b>93(81)</b>	<b>90(75)</b>	53(34)	19(7)	8(2)	5(0)	5(0)	6(0)
$S_3$	5(1)	5(1)	6(0)	6(0)	5(0)	4(0)	5(0)	4(0)	5(0)
(b) Simple scale change									
$M_g$ -NN	65(38)	74(46)	80(51)	<b>99(78)</b>	<b>94(68)</b>	<b>82(47)</b>	<b>98(70)</b>	<b>90(56)</b>	<b>81(46)</b>
GET	61(33)	71(40)	74(44)	<b>99(75)</b>	86(56)	69(35)	<b>97(68)</b>	83(46)	63(32)
MET	63(36)	72(42)	76(47)	<b>99(76)</b>	<b>91(63)</b>	76(42)	<b>98(68)</b>	<b>90(56)</b>	<b>77(43)</b>
SWR	5(0)	5(0)	5(0)	33(14)	19(7)	13(3)	23(10)	20(5)	12(3)
DM	63(36)	50(21)	32(4)	72(47)	57(34)	43(24)	4(0)	4(0)	4(0)
ED	5(2)	6(1)	6(1)	<b>98(78)</b>	<b>93(69)</b>	<b>83(56)</b>	30(12)	19(8)	18(6)
$C_{2N}$	73(41)	84(53)	<b>88(57)</b>	73(42)	66(27)	54(11)	5(0)	5(0)	4(0)
$S_3$	<b>83(54)</b>	<b>90(64)</b>	<b>92(67)</b>	66(42)	49(28)	37(19)	4(0)	4(0)	4(0)
(c) Complex scale change									
$M_g$ -NN	<b>96(73)</b>	<b>96(73)</b>	<b>95(72)</b>	<b>97(85)</b>	85(61)	70(39)	<b>95(80)</b>	86(67)	76(55)
GET	84(63)	79(56)	79(56)	90(76)	35(2)	14(1)	<b>96(84)</b>	77(61)	54(38)
MET	78(48)	77(44)	76(46)	81(60)	37(10)	24(1)	94(78)	83(64)	70(50)
SWR	80(61)	84(64)	82(64)	<b>96(84)</b>	<b>97(84)</b>	<b>96(83)</b>	<b>99(92)</b>	<b>98(88)</b>	<b>96(84)</b>
DM	8(0)	6(0)	7(0)	70(46)	70(43)	68(40)	5(0)	5(0)	5(0)
ED	10(2)	10(2)	8(2)	95(72)	97(74)	95(75)	5(1)	6(0)	4(1)
$C_{2N}$	7(1)	7(1)	7(2)	74(40)	77(27)	75(15)	5(0)	4(0)	6(0)
$S_3$	8(1)	9(1)	8(1)	67(43)	67(41)	66(39)	5(0)	5(0)	5(0)
(d) Location and simple scale mixed change									
$M_g$ -NN	69(44)	73(46)	80(53)	<b>69(48)</b>	<b>54(34)</b>	<b>37(21)</b>	<b>70(52)</b>	<b>60(43)</b>	<b>47(32)</b>
GET	64(37)	67(39)	76(46)	53(34)	28(13)	12(4)	37(24)	23(14)	16(8)
MET	66(39)	71(43)	77(49)	51(30)	28(12)	16(5)	49(32)	34(20)	28(14)
SWR	5(0)	5(0)	5(0)	13(3)	12(3)	11(3)	20(7)	22(8)	19(6)
DM	66(40)	47(19)	32(5)	14(4)	8(2)	7(1)	5(0)	4(0)	4(0)
ED	9(2)	9(3)	8(2)	60(39)	32(18)	19(6)	6(1)	5(1)	4(1)
$C_{2N}$	77(44)	83(54)	<b>89(61)</b>	37(16)	16(4)	10(2)	6(0)	5(0)	5(0)
$S_3$	<b>84(56)</b>	<b>88(63)</b>	<b>92(69)</b>	11(2)	7(1)	6(1)	5(0)	4(0)	4(0)
(e) Location and complex scale mixed change									
$M_g$ -NN	<b>84(56)</b>	<b>77(50)</b>	<b>74(45)</b>	<b>98(87)</b>	<b>96(84)</b>	<b>92(78)</b>	<b>78(59)</b>	<b>66(48)</b>	<b>54(39)</b>
GET	68(45)	60(37)	54(31)	<b>93(80)</b>	80(64)	57(43)	49(34)	31(20)	20(11)
MET	65(38)	58(30)	53(27)	<b>94(78)</b>	85(67)	67(50)	60(43)	46(29)	34(18)
SWR	47(24)	42(22)	42(21)	65(41)	68(47)	64(43)	29(13)	29(13)	30(13)
DM	8(0)	8(0)	7(0)	3(0)	5(0)	5(0)	5(0)	4(0)	5(0)
ED	40(25)	33(17)	25(12)	90(72)	62(46)	22(15)	6(1)	4(0)	4(1)
$C_{2N}$	40(20)	28(11)	22(8)	61(40)	22(10)	10(3)	5(0)	5(0)	6(0)
$S_3$	6(0)	8(1)	6(0)	4(0)	5(0)	5(0)	5(0)	4(0)	5(0)

In summary, the distance-based methods ED,  $C_{2N}$ , and  $S_3$ , as well as DM, are powerful for the light-tailed distribution. Specifically, ED exhibits superior power for the location alternative,  $S_3$  and DM are more powerful for the simple scale alternative, while  $C_{2N}$  covers both the location and the scale alternatives. Nevertheless, these methods suffer from outliers and are less powerful for heavy-tailed distributions. On the contrary, the graph-based methods GET and MET are less sensitive to outliers and show good performance for the complex scale alternative. The problem with these methods is that they use less information than distance-based methods, thus suffering from the lack of power for light-tailed distribution and the location alternative. In particular, SWR uses the least information compared to GET and MET, so it

has almost no power in many settings and alternatives when other methods attain moderate power. On the other hand,  $M_g$ -NN possesses good power for light-tailed distributions and shows robustness for heavy-tailed distributions.

## V. REAL DATA EXAMPLES

### A. Seizure detection from functional connectivity networks

We illustrate RING-CPD for identifying epileptic seizures, which over two million Americans are suffering from [67]. As a promising therapy, responsive neurostimulation requires automated algorithms to detect seizures as early as possible. Besides, to identify seizures, physicians have to review abundant electro-encephalogram (EEG) recordings,

TABLE IV  
THE EMPIRICAL POWER (DETECTION ACCURACY) IN PERCENT UNDER SETTINGS IV-VI. HERE  $M_g$ -NN IS THE PROPOSED METHOD.

d	Setting IV ( $\chi^2_5$ )			Setting V (Gaussian Mixture)			Setting VI (Gaussian outlier)		
	200	500	1000	200	500	1000	200	500	1000
(a) Location change									
$M_g$ -NN	74(56)	65(46)	54(37)	32(18)	42(27)	58(42)	61(44)	50(34)	42(24)
GET	60(43)	46(30)	33(21)	29(17)	39(25)	51(34)	44(30)	30(17)	21(9)
MET	64(47)	52(35)	39(25)	30(18)	41(28)	54(37)	48(33)	34(19)	27(13)
SWR	20(7)	18(6)	15(3)	20(6)	24(9)	31(13)	18(7)	15(4)	13(4)
DM	6(0)	5(0)	5(0)	7(0)	6(0)	7(0)	4(0)	6(0)	7(0)
ED	94(80)	93(79)	91(76)	6(1)	5(1)	6(1)	93(8)	90(73)	87(7)
$C_{2N}$	95(80)	92(78)	88(73)	87(53)	83(24)	84(11)	78(61)	44(26)	19(6)
$S_3$	5(1)	4(0)	6(1)	7(0)	6(0)	7(0)	4(0)	4(0)	6(0)
(b) Simple scale change									
$M_g$ -NN	90(64)	89(61)	86(58)	71(49)	81(58)	88(69)	84(61)	77(52)	70(47)
GET	85(57)	84(53)	80(51)	65(40)	76(51)	84(60)	87(61)	83(57)	75(51)
MET	88(61)	87(57)	83(54)	66(45)	76(55)	83(64)	85(59)	78(51)	72(44)
SWR	5(1)	6(0)	6(0)	5(0)	5(0)	5(1)	5(0)	5(0)	5(1)
DM	90(65)	82(52)	55(25)	6(0)	5(0)	5(0)	69(50)	59(40)	43(25)
ED	6(1)	8(2)	6(2)	5(1)	4(1)	5(1)	11(4)	13(4)	11(3)
$C_{2N}$	86(57)	91(63)	91(63)	6(1)	6(1)	6(0)	65(40)	56(31)	42(16)
$S_3$	93(68)	96(72)	96(72)	6(0)	5(0)	5(0)	53(38)	39(26)	24(14)
(c) Complex scale change									
$M_g$ -NN	74(49)	62(36)	58(33)	49(31)	42(28)	47(30)	72(50)	69(50)	66(47)
GET	57(40)	44(26)	37(20)	24(13)	18(9)	21(10)	44(28)	40(25)	37(24)
MET	52(29)	41(20)	36(15)	21(9)	15(6)	17(6)	45(27)	43(26)	44(25)
SWR	64(43)	63(43)	64 (42)	92(77)	92(79)	94(81)	58(36)	57(33)	57(34)
DM	4(0)	4(0)	4(0)	5(0)	5(0)	6(0)	5(1)	4(0)	4(0)
ED	8(1)	7(1)	8(1)	5(0)	5(1)	4(1)	8(1)	7(1)	7(0)
$C_{2N}$	3(0)	4(1)	5(0)	5(0)	5(0)	6(0)	5(0)	5(0)	6(0)
$S_3$	4(0)	4(0)	5(0)	5(0)	5(0)	6(0)	5(0)	5(0)	5(0)
(d) Location and simple scale mixed change									
$M_g$ -NN	70(42)	67(39)	63(38)	68(45)	81(56)	86(63)	86(62)	78(52)	74(47)
GET	66(37)	62(32)	58(31)	70(45)	81(56)	87(65)	93(71)	86(62)	80(60)
MET	66(39)	66(36)	60(34)	67(44)	79(57)	84(62)	88(64)	81(52)	75(50)
SWR	6(1)	5(0)	6(0)	7(1)	6(1)	7(1)	7(1)	8(2)	9(1)
DM	76(46)	57(27)	34(9)	7(0)	6(0)	6(0)	73(50)	59(37)	44(26)
ED	14(5)	10(3)	8(3)	5(1)	5(1)	4(1)	44(26)	38(22)	37(20)
$C_{2N}$	73(41)	77(44)	79(46)	52(22)	38(10)	38(5)	76(51)	57(32)	43(22)
$S_3$	82(54)	85(55)	85(56)	6(0)	6(0)	6(0)	55(38)	36(22)	24(14)
(e) Location and complex scale mixed change									
$M_g$ -NN	52(30)	41(23)	39(21)	42(25)	40(24)	45(29)	81(64)	76(59)	74(56)
GET	39(22)	25(12)	24(11)	19(9)	19(7)	20(10)	58(42)	49(32)	43(28)
MET	37(16)	26(11)	25(10)	15(6)	16(5)	18(7)	60(41)	52(34)	48(30)
SWR	42(22)	40(21)	40(19)	74(53)	76(54)	79(60)	56(33)	53(32)	50(29)
DM	4(0)	4(0)	5(0)	5(0)	5(0)	5(0)	4(0)	5(0)	4(0)
ED	10(2)	7(1)	7(1)	4(0)	5(1)	6(1)	43(25)	34(19)	28(14)
$C_{2N}$	8(2)	6(1)	5(0)	8(1)	9(1)	11(1)	20(9)	11(2)	4(0)
$S_3$	4(0)	4(0)	4(0)	5(0)	5(0)	5(0)	4(0)	6(0)	4(0)

which in some patients may be quite subtle. Hence, it is important to develop methods with low false positive and false negative rates to detect seizures from the EEG recordings. We use the “Detect seizures in intracranial EEG (iEEG) recordings” database by the UPenn and Mayo Clinic (<https://www.kaggle.com/c/seizure-detection>), which consists of the EEG recordings of 12 subjects (eight patients and four dogs). For each subject, both the normal brain activity and the seizure activity are recorded multiple times, which are one-second clips with various channels (from 16 to 72), reducing to a multivariate stream of iEEGs. Following the preprocessing procedure of [9], we represent the iEEG data as functional connectivity networks using Pearson correlation in the high-gamma band (70-100Hz) [68]. Functional con-

nnectivity networks are weighted graphs, where the vertices are the electrodes, and the weights of edges correspond to the coupling strength of the vertices. An illustration of the networks is in Figure 7. The sample sizes of the 12 subjects are also different, and the true change-points  $\tau$  are also known - before the change-point, the networks are from the seizure period, while after the change-point, the networks are from the normal brain activity, so we have the ground truth. We use the Frobenius norm to measure the distance between the observations represented by the weighted adjacency graphs.

We do not include SWR in the comparison here since SWR does not perform well in the simulation studies and is time-consuming. For  $C_{2N}$ , since it does well under some simulation settings, we try to include it in the comparison. However, it is

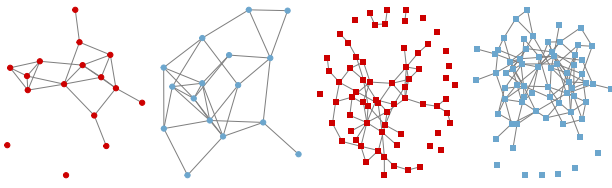


Fig. 7. The functional connectivity networks of a dog (circle) and a human (square) during the period of the seizure (red) and the normal period (blue). The networks are drawn by only keeping the edges with weights larger than 0.2.

TABLE V

THE ABSOLUTE DIFFERENCE BETWEEN THE TRUE CHANGE-POINT AND THE DETECTED CHANGE-POINT ( $|\hat{\tau} - \tau|$ ). THE  $p$ -VALUES OF ALL METHODS FOR ALL SUBJECTS (DOGS OR PTs, WHERE PT= PATIENT) ARE SMALLER THAN 0.01.  $M_g$ -NN IS THE PROPOSED METHOD.

	$n$	$\tau$	$M_g$ -NN	MET	DM	ED	$C_{2N}$	$S_3$
Dog 1	596	178	0	0	0	1	0	0
Dog 2	1320	172	4	4	1	3	-	1
Dog 3	5240	480	0	0	1	1	-	1
Dog 4	3047	257	3	3	3	2	-	3
PT 1	174	70	1	1	1	0	7	1
PT 2	3141	151	7	7	13	1	-	13
PT 3	1041	327	0	0	162	1	-	162
PT 4	210	20	0	0	67	11	137	67
PT 5	2745	135	3	3	5	2	-	5
PT 6	2997	225	0	0	0	1	-	0
PT 7	3521	282	2	2	3	4	-	3
PT 8	1890	180	0	0	0	1	-	0

not only time-consuming but also memory-consuming (e.g., it requires at least 17Gb size of memory when  $n = 1320$ ); we are only able to run it for  $n \leq 600$ , thus only showing its result for Dog 1, and Patients 1 and 4. Since the sample size of each subject is large enough, we use the asymptotic  $p$ -value approximation for  $M_g$ -NN and MET. We omit the result of GET since it performs similarly to MET but its  $p$ -value approximation is not as exact as MET. For DM, ED, and  $S_3$ , we still use 1,000 random permutations to obtain the  $p$ -values. The results are summarized in Table V, where the absolute difference between the true change-point and the detected change-point  $|\hat{\tau} - \tau|$  is reported. The  $p$ -values are not reported as they are smaller than 0.01 for all methods and subjects. Our method achieves the same detection error as MET, which is very small for all subjects. ED also performs well, but with a slightly large error for Patient 4. Although DM and  $S_3$  achieve small errors for most subjects, they attain large detection errors for Patients 3 and 4. The performance of  $C_{2N}$  is not robust in that it shows a large detection error for Patient 4.

### B. Change-point detection for MNIST handwritten digits

To better demonstrate the efficacy of RING-CPD on non-Euclidean datasets, we evaluated its performance using the MNIST dataset of handwritten digits [69]. The MNIST dataset comprises images of digits ranging from 0 to 9, with each image being a  $28 \times 28$  matrix. Each matrix element represents a grayscale intensity value between 0 and 255. For our analysis, we select image pairs that are typically challenging to differentiate: digits 0 and 8, 1 and 7, 5 and 6, 3 and 8, and

4 and 9. We structure the dataset such that the first  $\tau$  images correspond to one digit and the remaining  $n - \tau$  images to another, with configurations  $(\tau, n) = (15, 30)$  and  $(15, 45)$ . A nominal level  $\alpha = 0.05$  is used, and each scenario is repeated 100 times through random sampling of images. The negative Frobenius norm serves as the similarity measure.

We present the empirical power (defined as the proportion of trials with a  $p$ -value less than 0.05) in Table VI with the average change-point estimation error  $|\tau - \hat{\tau}|$  for those rejecting  $H_0$  in parentheses. Notably, the traditional Euclidean distance-based method ED is ineffective across all scenarios, evidenced by a zero empirical detection rate, so we omit its results in Table VI. In contrast,  $M_g$ -NN demonstrates superior performance in nearly all configurations. Other graph-based methodologies like GET, MET, and SWR also perform commendably. However, methods such as DM,  $C_{2N}$ , and  $S_3$  perform unsatisfactorily in some scenarios, likely due to the sparse and complex nature of image data.

### C. Changed interval detection for New York taxi data

We illustrate our method for changed interval detection in studying travel pattern changes around New York Central Park. We use the yellow taxi trip records for the year 2014 available on the the NYC Taxi and Limousine Commission (TLC) website (<https://www1.nyc.gov/site/tlc/about/tlc-trip-record-data.page>), which contains the city's taxi pickup and drop-off times and locations (longitude and latitude coordinates). We set the latitude range of New York Central Park as 40.76 to 40.81 and the longitude range as -74.10 to -73.60. The boundary of New York City is set as 40.50 to 40.95 in latitude and -74.10 to -73.60. We only consider those trips that began with a pickup in New York City and ended with a drop-off in New York Central Park. We use the two-dimensional kernel density estimation with the bivariate normal kernel and 50 grid points in each direction to represent the trips of each day in New York City, as illustrated by Figure 8 on two random days. We use the Frobenius norm to construct the similarity graphs in the subsequent analysis. The  $p$ -values of all methods are obtained through 1000 random permutations.

We first compare RING-CPD with GET and MET. We set  $n_0 = \max\{5, [0.05n]\}$ ,  $n_1 = n - n_0$ , and the nominal level to be 0.01. All methods detect the same changed interval 06/19-08/31 with  $p$ -values  $< 0.001$ , which almost entirely overlaps with the summer break. Besides, 06/19 is Juneteenth and 09/01 is Labor Day.

Since there may be multiple changed intervals, we apply the methods recursively. Specifically, we apply the methods to the three segments divided by the detected changed interval. For the period of 01/01-06/18, all methods detect the changed interval 03/18-03/28 with  $p$ -value  $< 0.001$ , which is around the spring break period for most American universities, while 3/17 is St. Patrick's Day. For the period of 06/19-08/31, no method can reject the null hypothesis at the 0.01 significance level. For the period of 09/01-12/31,  $M_g$ -NN, GET, and MET report the changed interval starting at 09/01, 09/03, and 09/02 respectively and all ending at 11/12 with  $p$ -values

TABLE VI

THE EMPIRICAL POWER WITH THE AVERAGE CHANGE-POINT ESTIMATION ERROR IN PARENTHESES.  $M_g$ -NN IS THE PROPOSED METHOD. THE METHOD WITH THE HIGHEST EMPIRICAL POWER IS HIGHLIGHTED IN BOLD. IF TWO METHODS HAVE THE SAME POWER, CHOOSE THE ONE WITH THE SMALLER AVERAGE CHANGE-POINT ESTIMATION ERROR.

Setting	$M_g$ -NN	GET	MET	SWR	DM	$C_{2N}$	$S_3$
$(\tau, n) = (15, 30)$	0/8 <b>1.00 (0.06)</b>	1.00 (0.10)	1.00 (0.10)	0.99 (0.09)	0.90 (0.20)	1.00 (4.38)	0.96 (0.17)
	1/7 <b>1.00 (0.07)</b>	<b>1.00 (0.07)</b>	<b>1.00 (0.07)</b>	1.00 (0.10)	0.99 (0.13)	1.00 (3.29)	1.00 (0.10)
	5/6 <b>1.00 (0.20)</b>	1.00 (0.43)	1.00 (0.43)	0.99 (0.29)	0.37 (2.79)	1.00 (2.79)	0.30 (1.60)
	3/8 <b>0.98 (0.89)</b>	0.93 (0.98)	0.96 (1.04)	0.78 (1.17)	0.22 (8.91)	0.96 (2.16)	0.15 (4.00)
	4/9 <b>0.61 (1.08)</b>	0.54 (1.78)	0.51 (1.43)	0.56 (2.34)	0.13 (10.62)	0.62 (2.39)	0.04 (13.00)
$(\tau, n) = (15, 45)$	0/8 <b>1.00 (0.02)</b>	1.00 (0.05)	1.00 (0.05)	1.00 (0.16)	1.00 (0.38)	1.00 (8.90)	1.00 (0.20)
	1/7 1.00 (0.09)	1.00 (0.16)	1.00 (0.13)	<b>1.00 (0.07)</b>	1.00 (0.20)	1.00 (2.69)	1.00 (0.17)
	5/6 <b>1.00 (0.17)</b>	1.00 (0.38)	1.00 (0.46)	1.00 (0.39)	0.76 (3.72)	1.00 (7.02)	0.96 (0.75)
	3/8 <b>1.00 (0.45)</b>	1.00 (0.55)	1.00 (0.55)	0.98 (1.63)	0.52 (7.37)	1.00 (4.30)	0.81 (1.30)
	4/9 <b>0.86 (1.55)</b>	0.80 (2.33)	0.77 (2.68)	0.70 (2.76)	0.11 (16.00)	0.79 (2.88)	0.18 (6.89)

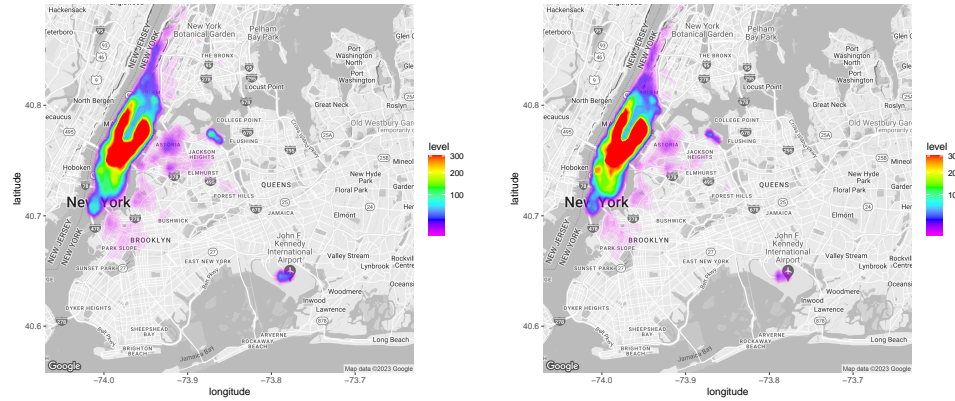


Fig. 8. Density heatmap of taxi pick-ups for dates 01/01 and 02/01 in year 2014.

$< 0.001$ . This is the changed interval of the Fall Semester till Veterans Day (11/11).

We further apply these methods to the segments that are longer than 40 days. The only detected changed interval is 01/27-01/31 reported by  $M_g$ -NN with  $p$ -value 0.01 in the segment 01/01-03/17, which is around the Lunar New Year

(01/31/2014). It is worth noting that for the period of 11/13-12/31, all methods report the changed interval that covers Christmas, while  $M_g$ -NN yields a small  $p$ -value 0.02 and other methods report  $p$ -values larger than 0.05. The results are summarized in Table VII.

We also apply other methods to the dataset. Since both

TABLE VII  
THE DETECTED CHANGED INTERVALS AND CORRESPONDING  $p$ -VALUES OF  $M_g$ -NN, GET AND MET FOR THE NYC TAXI DATA.

Time period	$M_g$ -NN	GET	MET	Nearby Events
01/01-12/31 $p$ -value	<b>06/19-08/31</b> $< 0.001$			Summer break
01/01-06/18 $p$ -value	<b>03/18-03/28</b> $< 0.001$			Spring break/St. Patrick's Day
06/19-08/31 $p$ -value	06/23-06/27 0.048	07/17-08/29 0.196	06/23-06/27 0.223	-
09/01-12/31 $p$ -value	<b>09/01-11/12</b> $< 0.001$	<b>09/03-11/12</b> $< 0.001$	<b>09/02-11/12</b> $< 0.001$	Fall Semester (till Veterans Day)
01/01-03/17 $p$ -value	<b>01/27-01/31</b> 0.01	02/19-03/13 0.051	02/19-03/13 0.263	Lunar New Year
03/29-06/18 $p$ -value	04/04-06/15 0.094	04/23-05/22 0.366	04/23-05/23 0.333	-
09/01(03, 02)-11/12 $p$ -value	09/02-09/11 0.014	09/03-09/11 0.073	09/02-09/12 0.028	-
11/13-12/31 $p$ -value	12/22-12/30 0.020	12/20-12/30 0.067	12/20-12/30 0.059	-
02/01-03/17 $p$ -value	03/03-03/07 0.263			-

TABLE VIII  
THE DETECTED CHANGE-POINTS AND CORRESPONDING  $p$ -VALUES OF ED,  
 $S_3$  AND  $C_{2N}$  FOR THE NYC TAXI DATA.

Method	ED	$S_3$	$C_{2N}$	
CP	06/20	09/02	06/20	06/19
$p$ -value	0.001	0.001	0.003	< 0.001
				0.004

ED and  $S_3$  can detect multiple change points, we apply them directly to the whole sequence 01/01-12/31. We also include  $C_{2N}$ . Although  $C_{2N}$  is not designed for multiple change-point detections, we adopt the same binary segmentation procedure used by  $S_3$  [34]. As summarized in Table VIII, ED detects two change-points 06/20 and 09/02 both with  $p$ -values 0.001.  $S_3$  only detects one change-point 06/20 with  $p$ -value 0.003.  $C_{2N}$  detects two change-points, which are 06/19 and 09/14, with  $p$ -values < 0.001 and 0.004. They all miss some important change points shown in Table VIII.

## VI. DISCUSSION

### A. Kernel and Distance IN Graph CPD

The proposed approach can be extended to use weights other than ranks in weighting the edges in the similarity graph. For example, we could incorporate kernel value or distance directly to have Kernel IN Graph Change-Point Detection (KING-CPD) and Distance IN Graph Change-Point Detection (DING-CPD) methods. Specifically, we can use the kernel values or (negative) pairwise distances to weight the similarity graph, and the asymptotic property still holds under mild conditions. Let

$$K_{ij} = K(y_i, y_j) \mathbb{1}((i, j) \in G_k),$$

where  $K$  is a kernel function or a negative distance function, for example, the Gaussian kernel  $K(y_i, y_j) = \exp(-\|y_i - y_j\|^2/(2\sigma^2))$  with the kernel bandwidth  $\sigma$  or  $K(y_i, y_j)$  simply the negative  $l_1$  distance  $K(y_i, y_j) = -\|y_i - y_j\|_1$ , and  $G_k$  is a similarity graph such as the  $k$ -NNG or the  $k$ -MST. We require Condition (7)  $\max_{i,j} K_{ij} = o(n^2 r_d^2)$ , which essentially states that there is no element of  $K_{ij}$  dominates others.

**Theorem 4:** Replacing  $R_{ij}$  by  $K_{ij}$  in Conditions (1)-(6), and the definition of  $Z_{\text{diff}}$  and  $Z_w$ , then under Conditions (1)-(6) and (7), we have

- 1)  $\{Z_{\text{diff}}(\lfloor nu \rfloor) : 0 < u < 1\}$  and  $\{Z_w(\lfloor nu \rfloor) : 0 < u < 1\}$  converge to independent Gaussian processes in finite-dimensional distributions, which we denote as  $\{Z_{\text{diff}}^*(u) : 0 < u < 1\}$  and  $\{Z_w^*(u) : 0 < u < 1\}$ , respectively.
- 2)  $\{Z_{\text{diff}}(\lfloor nu \rfloor, \lfloor nv \rfloor) : 0 < u < v < 1\}$  and  $\{Z_w(\lfloor nu \rfloor, \lfloor nv \rfloor) : 0 < u < v < 1\}$  converge to independent two-dimension Gaussian random fields in finite-dimensional distributions, which we denote as  $\{Z_{\text{diff}}^*(u, v) : 0 < u < v < 1\}$  and  $\{Z_w^*(u, v) : 0 < u < v < 1\}$ , respectively.

In addition, Theorem 2 also holds by replacing  $R_{ij}$  by  $K_{ij}$ .

The proof of Theorem 4 follows straightforwardly from the proof of Theorems 1 and 2, thus omitted here.

## ACKNOWLEDGMENTS

The authors would like to thank the associate editor and referees for their constructive comments and suggestions.

## REFERENCES

- [1] E. S. Page, "Continuous inspection schemes," *Biometrika*, vol. 41, no. 1/2, pp. 100–115, 1954.
- [2] F. Desobry, M. Davy, and C. Doncarli, "An online kernel change detection algorithm," *IEEE Transactions on Signal Processing*, vol. 53, no. 8, pp. 2961–2974, 2005.
- [3] A. G. Tartakovsky and V. V. Veeravalli, "Asymptotically optimal quickest change detection in distributed sensor systems," *Sequential Analysis*, vol. 27, no. 4, pp. 441–475, 2008.
- [4] Y. Xie and D. Siegmund, "Sequential multi-sensor change-point detection," in *2013 Information Theory and Applications Workshop (ITA)*. IEEE, 2013, pp. 1–20.
- [5] H. Chen, "Sequential change-point detection based on nearest neighbors," *The Annals of Statistics*, vol. 47, no. 3, pp. 1381–1407, 2019.
- [6] L. Xie, Y. Xie, and G. V. Moustakides, "Sequential subspace change point detection," *Sequential Analysis*, vol. 39, no. 3, pp. 307–335, 2020.
- [7] L. Chu and H. Chen, "Sequential change-point detection for high-dimensional and non-euclidean data," *IEEE Transactions on Signal Processing*, vol. 70, pp. 4498–4511, 2022.
- [8] I. Barnett and J.-P. Onnela, "Change point detection in correlation networks," *Scientific Reports*, vol. 6, no. 1, pp. 1–11, 2016.
- [9] D. Zambon, C. Alippi, and L. Livi, "Change-point methods on a sequence of graphs," *IEEE Transactions on Signal Processing*, vol. 67, no. 24, pp. 6327–6341, 2019.
- [10] M. Staudacher, S. Telser, A. Amann, H. Hinterhuber, and M. Ritsch-Marte, "A new method for change-point detection developed for on-line analysis of the heart beat variability during sleep," *Physica A: Statistical Mechanics and its Applications*, vol. 349, no. 3-4, pp. 582–596, 2005.
- [11] R. Malladi, G. P. Kalamangalam, and B. Aazhang, "Online bayesian change point detection algorithms for segmentation of epileptic activity," in *2013 Asilomar Conference on Signals, Systems and Computers*. IEEE, 2013, pp. 1833–1837.
- [12] G. Kossinets and D. J. Watts, "Empirical analysis of an evolving social network," *Science*, vol. 311, no. 5757, pp. 88–90, 2006.
- [13] N. Eagle, A. S. Pentland, and D. Lazer, "Inferring friendship network structure by using mobile phone data," *Proceedings of the National Academy of Sciences*, vol. 106, no. 36, pp. 15 274–15 278, 2009.
- [14] L. Peel and A. Clauset, "Detecting change points in the large-scale structure of evolving networks," in *Twenty-Ninth AAAI Conference on Artificial Intelligence*, 2015.
- [15] J. Bai and P. Perron, "Estimating and testing linear models with multiple structural changes," *Econometrica*, pp. 47–78, 1998.
- [16] M. Talih and N. Hengartner, "Structural learning with time-varying components: tracking the cross-section of financial time series," *Journal of the Royal Statistical Society: Series B (Statistical Methodology)*, vol. 67, no. 3, pp. 321–341, 2005.
- [17] M. Srivastava and K. J. Worsley, "Likelihood ratio tests for a change in the multivariate normal mean," *Journal of the American Statistical Association*, vol. 81, no. 393, pp. 199–204, 1986.
- [18] N. R. Zhang, D. O. Siegmund, H. Ji, and J. Z. Li, "Detecting simultaneous changepoints in multiple sequences," *Biometrika*, vol. 97, no. 3, pp. 631–645, 2010.
- [19] D. Siegmund, B. Yakir, and N. R. Zhang, "Detecting simultaneous variant intervals in aligned sequences," *The Annals of Applied Statistics*, vol. 5, no. 2A, pp. 645–668, 2011.
- [20] J. Chen and A. K. Gupta, *Parametric statistical change point analysis: with applications to genetics, medicine, and finance*. Springer, 2012.
- [21] G. Wang, C. Zou, and G. Yin, "Change-point detection in multinomial data with a large number of categories," *The Annals of Statistics*, vol. 46, no. 5, pp. 2020–2044, 2018.
- [22] S. Li, Y. Xie, H. Dai, and L. Song, "M-statistic for kernel change-point detection," *Advances in Neural Information Processing Systems*, vol. 28, 2015.
- [23] D. Garreau and S. Arlot, "Consistent change-point detection with kernels," *Electronic Journal of Statistics*, vol. 12, no. 2, pp. 4440–4486, 2018.
- [24] S. Arlot, A. Celisse, and Z. Harchaoui, "A kernel multiple change-point algorithm via model selection," *Journal of Machine Learning Research*, vol. 20, no. 162, 2019.

[25] W.-C. Chang, C.-L. Li, Y. Yang, and B. Póczos, “Kernel change-point detection with auxiliary deep generative models,” in *International Conference on Learning Representations*, 2019.

[26] D. S. Matteson and N. A. James, “A nonparametric approach for multiple change point analysis of multivariate data,” *Journal of the American Statistical Association*, vol. 109, no. 505, pp. 334–345, 2014.

[27] J. Li, “Asymptotic distribution-free change-point detection based on interpoint distances for high-dimensional data,” *Journal of Nonparametric Statistics*, vol. 32, no. 1, pp. 157–184, 2020.

[28] H. Chen and N. Zhang, “Graph-based change-point detection,” *The Annals of Statistics*, vol. 43, no. 1, pp. 139–176, 2015.

[29] X. Shi, Y. Wu, and C. R. Rao, “Consistent and powerful graph-based change-point test for high-dimensional data,” *Proceedings of the National Academy of Sciences*, vol. 114, no. 15, pp. 3873–3878, 2017.

[30] L. Chu and H. Chen, “Asymptotic distribution-free change-point detection for multivariate and non-euclidean data,” *The Annals of Statistics*, vol. 47, no. 1, pp. 382–414, 2019.

[31] H. Chen, “Change-point detection for multivariate and non-euclidean data with local dependency,” *arXiv preprint arXiv:1903.01598*, 2019.

[32] H. Song and H. Chen, “Asymptotic distribution-free changepoint detection for data with repeated observations,” *Biometrika*, vol. 109, no. 3, pp. 783–798, 2022.

[33] Y.-W. Liu and H. Chen, “A fast and efficient change-point detection framework based on approximate  $k$ -nearest neighbor graphs,” *IEEE Transactions on Signal Processing*, vol. 70, pp. 1976–1986, 2022.

[34] L. Nie and D. L. Nicolae, “Weighted-graph-based change point detection,” *arXiv preprint arXiv:2103.02680*, 2021.

[35] H. Chen and L. Chu, “Graph-based change-point analysis,” *Annual Review of Statistics and Its Application*, vol. 10, no. 1, pp. 475–499, 2023.

[36] L. Chu and H. Chen, “On the tightness of graph-based statistics,” *Electronic Journal of Statistics*, vol. 19, no. 1, pp. 1425–1452, 2025.

[37] H. Chen and J. H. Friedman, “A new graph-based two-sample test for multivariate and object data,” *Journal of the American Statistical Association*, vol. 112, no. 517, pp. 397–409, 2017.

[38] G. K. Bhattacharyya and R. A. Johnson, “Nonparametric tests for shift at an unknown time point,” *The Annals of Mathematical Statistics*, pp. 1731–1743, 1968.

[39] B. Darkhovskh, “A nonparametric method for the a posteriori detection of the “disorder” time of a sequence of independent random variables,” *Theory of Probability & Its Applications*, vol. 21, no. 1, pp. 178–183, 1976.

[40] A. N. Pettitt, “A non-parametric approach to the change-point problem,” *Journal of the Royal Statistical Society: Series C (Applied Statistics)*, vol. 28, no. 2, pp. 126–135, 1979.

[41] E. Schectman, “A nonparametric test for detecting changes in location,” *Communications in Statistics-Theory and Methods*, vol. 11, no. 13, pp. 1475–1482, 1982.

[42] F. Lombard, “Rank tests for changepoint problems,” *Biometrika*, vol. 74, no. 3, pp. 615–624, 1987.

[43] —, “Asymptotic distributions of rank statistics in the change-point problem,” *South African Statistical Journal*, vol. 17, no. 1, pp. 83–105, 1983.

[44] C. Gerstenberger, “Robust wilcoxon-type estimation of change-point location under short-range dependence,” *Journal of Time Series Analysis*, vol. 39, no. 1, pp. 90–104, 2018.

[45] Y. Wang, Z. Wang, and X. Zi, “Rank-based multiple change-point detection,” *Communications in Statistics-Theory and Methods*, vol. 49, no. 14, pp. 3438–3454, 2020.

[46] A. Lung-Yut-Fong, C. Lévy-Leduc, and O. Cappé, “Homogeneity and change-point detection tests for multivariate data using rank statistics,” *Journal de la Société Française de Statistique*, vol. 156, no. 4, pp. 133–162, 2015.

[47] C. Zhang, N. Chen, and J. Wu, “Spatial rank-based high-dimensional monitoring through random projection,” *Journal of Quality Technology*, vol. 52, no. 2, pp. 111–127, 2020.

[48] L. Shu, Y. Chen, W. Zhang, and X. Wang, “Spatial rank-based high-dimensional change point detection via random integration,” *Journal of Multivariate Analysis*, vol. 189, p. 104942, 2022.

[49] S. Chenouri, A. Mozaffari, and G. Rice, “Robust multivariate change point analysis based on data depth,” *Canadian Journal of Statistics*, vol. 48, no. 3, pp. 417–446, 2020.

[50] D. Zhou and H. Chen, “A new ranking scheme for modern data and its application to two-sample hypothesis testing,” in *The Thirty Sixth Annual Conference on Learning Theory*. PMLR, 2023, pp. 3615–3668.

[51] Y. Zhang and H. Chen, “Graph-based multiple change-point detection,” *arXiv preprint arXiv:2110.01170*, 2021.

[52] P. Fryzlewicz, “Wild binary segmentation for multiple change-point detection,” *The Annals of Statistics*, vol. 42, no. 6, pp. 2243–2281, 2014.

[53] S. Kovács, P. Bühlmann, H. Li, and A. Munk, “Seeded binary segmentation: a general methodology for fast and optimal changepoint detection,” *Biometrika*, vol. 110, no. 1, pp. 249–256, 2023.

[54] J. H. Friedman and L. C. Rafsky, “Multivariate generalizations of the Wald-Wolfowitz and Smirnov two-sample tests,” *The Annals of Statistics*, pp. 697–717, 1979.

[55] J. L. Bentley, “Multidimensional binary search trees used for associative searching,” *Communications of the ACM*, vol. 18, no. 9, pp. 509–517, 1975.

[56] S. M. Omohundro, “Five balltree construction algorithms,” International Computer Science Institute, Berkeley, CA, Technical Report TR-89-063, 1989.

[57] F. Pedregosa, G. Varoquaux, A. Gramfort, V. Michel, B. Thirion, O. Grisel, M. Blondel, P. Prettenhofer, R. Weiss, V. Dubourg, J. Vanderplas, A. Passos, D. Cournapeau, M. Brucher, M. Perrot, and Édouard Duchesnay, “Scikit-learn: Machine learning in python,” *Journal of Machine Learning Research*, vol. 12, no. 85, pp. 2825–2830, 2011.

[58] P. Ram and K. Sinha, “Revisiting kd-tree for nearest neighbor search,” in *Proceedings of the 25th ACM SIGKDD International Conference on Knowledge Discovery & Data Mining*, 2019, pp. 1378–1388.

[59] S. Arya, D. M. Mount, N. S. Netanyahu, R. Silverman, and A. Y. Wu, “An optimal algorithm for approximate nearest neighbor searching fixed dimensions,” *Journal of the ACM (JACM)*, vol. 45, no. 6, pp. 891–923, 1998.

[60] M. Woodroofe, “Frequentist properties of bayesian sequential tests,” *Biometrika*, vol. 63, no. 1, pp. 101–110, 1976.

[61] —, “Large deviations of likelihood ratio statistics with applications to sequential testing,” *The Annals of Statistics*, pp. 72–84, 1978.

[62] D. Siegmund, “Approximate tail probabilities for the maxima of some random fields,” *The Annals of Probability*, pp. 487–501, 1988.

[63] —, “Tail approximations for maxima of random fields,” in *Probability Theory: Proceedings of the 1989 Singapore Probability Conference*. Singapore, 1992, pp. 147–158.

[64] D. Siegmund and B. Yakir, *The statistics of gene mapping*. Springer Science & Business Media, 2007.

[65] N. Henze and M. D. Penrose, “On the multivariate runs test,” *Annals of Statistics*, pp. 290–298, 1999.

[66] P. Dubey and H.-G. Müller, “Fréchet change-point detection,” *The Annals of Statistics*, vol. 48, no. 6, pp. 3312–3335, 2020.

[67] L. D. Iasemidis, “Epileptic seizure prediction and control,” *IEEE Transactions on Biomedical Engineering*, vol. 50, no. 5, pp. 549–558, 2003.

[68] A. M. Bastos and J.-M. Schoffelen, “A tutorial review of functional connectivity analysis methods and their interpretational pitfalls,” *Frontiers in Systems Neuroscience*, vol. 9, p. 175, 2016.

[69] Y. LeCun, L. Bottou, Y. Bengio, and P. Haffner, “Gradient-based learning applied to document recognition,” *Proceedings of the IEEE*, vol. 86, no. 11, pp. 2278–2324, 1998.

**Doudou Zhou** received his Ph.D. in Statistics from the University of California, Davis, in 2022. From 2022 to 2024, he was a Postdoctoral Researcher at Harvard University. He is currently an Assistant Professor in the Department of Statistics and Data Science at the National University of Singapore. His research focuses on developing theoretical and computational methods for high-dimensional data analysis and machine learning.

**Hao Chen** received her Ph.D. in Statistics from Stanford University in 2013. Since then, she joined the Department of Statistics, University of California, Davis, as a faculty member, where she is currently an Associate Professor (with tenure). Her research interests include developing practical and robust methods that can deal with various data types, including high-dimensional data, image data, and network data, for hypothesis testing, signal detection, classification, and clustering.